

Tubular Micro/Nanomachines: From the Basics to Recent Advances

Borui Xu, Biran Zhang, Lu Wang, Gaoshan Huang, and Yongfeng Mei*

Inspired by the machines that have changed the world through their autonomous functions, scientists have focused their attention on performing similar functions at the micro/nanoscale. The motility of these micro/nanomachines (micro/nanomotors) offers enormous opportunities for cargo delivery, biodection, and environmental and biomedical applications. Among the various geometries of micro/nanomotors, a tubular shape provides asymmetric inner and outer surfaces, where the inner wall hosts chemical reactions that supply the moving power and the outer wall can be modified for specific chemical and biological functions. This review describes the concept of tubular micro/nanomotors, including their basic principles, fabrication methods and control over their motion. With the assistance of catalytic reactions, tubular micro/nanomotors can generate a powerful thrust force to navigate in complex natural and in vitro environments. Modification of the tubular micro/nanomotors allows the motors to capture, transport, and release selected cargos on demand. In addition, their application in sensing and decontamination benefits from their collection behavior and self-mixing effect. Furthermore, noncatalytic reaction-driven tubular micro/nanomotors, such as redox-based and biohybrid tubular micro/nanomotors, provide new possibilities for practical in vivo applications. The state-of-the-art tubular micro/nanomotors could offer a promising platform for various applications, e.g., lab-on-chip devices and in vivo theranostics.

Since that speech, considerable effort has been devoted to research on micro/nanomachines. One important issue that urgently needs to be solved is the power source for micro/nanomachines. Different strategies have been advanced to obtain power from chemical reactions or biological motion. Currently, micro/nanomachines that are capable of moving, called micro/nanomotors, can complete several tasks at the microscale ranging from carrying, transporting, and releasing cargos to detecting and analyzing molecules as well as interacting with biological cells.

With the development of nanotechnology, different geometries of micro/nanomotors, including Janus particles,^[4] rods,^[5] helices,^[6] and biomimetic shapes,^[7] have been developed with the goal of realizing functional micro/nanomachines.^[8] Rocket-shaped tubular micro/nanomotors have attracted substantial attention due to their asymmetric inner and outer surfaces. The inner wall commonly consists of catalysts or reactive materials that can provide thrust, while the outer wall can be modified

with chemical or biological materials to endow the micro/nanomotors with the ability to conduct specific functions. In this review, the basics of tubular micro/nanomotors are introduced, including their working principles, mechanisms of propulsion, fabrication methods, and control strategies. Tubular micro/nanomotors based on catalytic reactions and their applications in cargo delivery, biosensing, and environmental remediation are reviewed. Meanwhile, other noncatalytic reaction-driven tubular micro/nanomotors that have achieved in vivo biomedical applications are introduced. Finally, a summary and outlook for the possible direction of future development are given.

1. Introduction

Machines that use chemical, thermal, or electrical power to perform designed functions and complete specific tasks have promoted all aspects of society and human life. The invention of steam-powered machines triggered the Industrial Revolution.^[1] Later, the production of the internal combustion engine marked a major turning point in the Technological Revolution,^[2] and this engine still functions in industry and our daily lives. Currently, we are surrounded by many types of machines and cannot live without their assistance. As noted by Feynman in his famous speech in 1959,^[3] the miniaturization of machines to the micro/nanoscale would open a new era in technology.

2. Tubular Micro/Nanomotors at Low Reynolds Numbers

Micro/nanomotors^[8a,9] are also regarded as engines,^[10] jets,^[11] rockets,^[12] and robots^[13] at the micro/nanoscale. Specifically, micro/nanojets and rockets are used to describe tubular micro/nanomotors that possess similar shapes and propulsion mechanisms as jets and rockets in the real world. These jets and rockets can generate substantial thrust to overcome gravity

B. R. Xu, B. R. Zhang, L. Wang, Prof. G. S. Huang, Prof. Y. F. Mei
Department of Materials Science
State Key Laboratory of ASIC and Systems
Fudan University
Shanghai 200433, China
E-mail: yfm@fudan.edu.cn

 The ORCID identification number(s) for the author(s) of this article can be found under <https://doi.org/10.1002/adfm.201705872>.

DOI: 10.1002/adfm.201705872

and propel themselves away from the ground into the sky or space. However, at the micro/nanoscale, the motion of micro/nanomotors in a liquid at low Reynolds numbers is mainly hampered by viscous force and the Brownian motion of the surrounding liquid molecules, as described by Purcell in 1976.^[14] The Reynolds number, which was introduced by Sir George Stokes and popularized by Osborne Reynolds to describe the transition of a fluid's flow from laminar flow to turbulent flow, is defined as the ratio of inertial forces to viscous force as follows: $Re = \rho ul/\mu$, where ρ , u , l , μ are the density of the fluid, the velocity of the fluid relative to the moving object, the characteristic length of the object, and the dynamic viscosity of the fluid, respectively. For an object moving in a fluid, the Reynolds number enables us to quantitatively distinguish the forces that dominate the motion (Figure 1). For an object moving at the macroscale, such as a swimmer, the Reynolds number can be up to 10^4 . For smaller objects, e.g., goldfish, the Reynolds number is $\approx 10^2$. In these cases, the large Reynolds numbers indicate that the inertial force is much greater than the viscous force. However, for objects moving at the microscale, for example, an *Escherichia coli* (*E. coli*) bacterium, the Reynolds number can be much smaller. The average mean speed of *E. coli* is $30 \mu\text{m s}^{-1}$, and it has a radius of $\approx 1 \mu\text{m}$ with a length of $\approx 2 \mu\text{m}$. The viscosity of water is $\approx 1 \text{ mPa s}$. Therefore, the Reynolds number of an *E. coli* bacterium is $\approx 10^{-4}$. This value implies that viscous force dominates the motion and that the influence of inertial force can be neglected for microscale objects.

To realize the directional movement of micro/nanomotors, a variety of strategies^[15] have been developed, including the utilization of an external energy supply (e.g., electric,^[16]

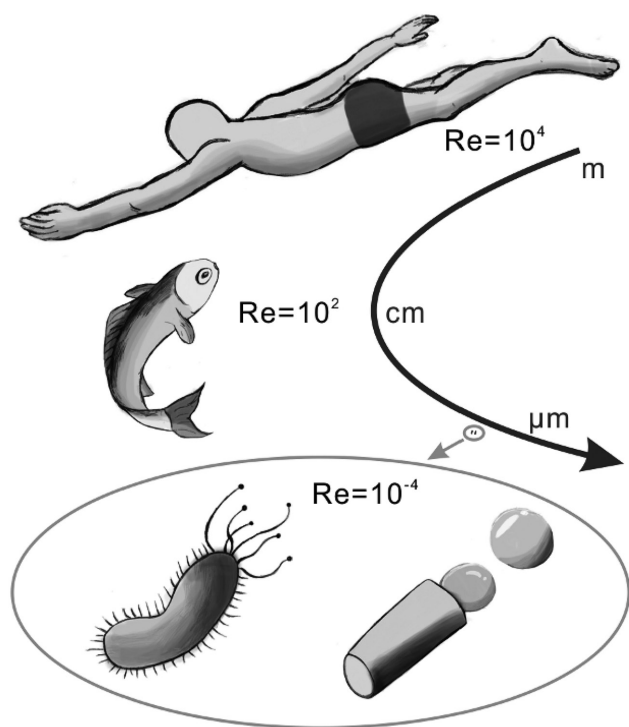


Figure 1. Swimming objects with different sizes and Reynolds numbers (from top to bottom: swimmer, fish, bacteria, and artificial tubular micro/nanomotor).



functionalization with smart materials.

Borui Xu is a Ph.D. student in the Department of Materials Science at Fudan University, under the supervision of Professor Yongfeng Mei. He received his B.S. in materials science from Fudan University in 2014. His research is focused on the development of micro/nanotubes fabricated by rolled-up nanotechnology and their



Biran Zhang is an M.S. student in the Department of Material Science at Fudan University, under the supervision of Professor Yongfeng Mei. She received her B.S. at Fudan University in 2016. Her research focuses on the motion control of tubular micro/nanomotors.



research group in the Leibniz Institute for Solid State and Materials Research Dresden as a staff scientist.

Yongfeng Mei received his B.S. and M.S. in physics from Nanjing University and Ph.D. in physics and materials science from City University of Hong Kong. He is a professor in materials chemistry and physics at Fudan University. Before that, he worked as a postdoctoral researcher in the Max Planck Institute for Solid State Research and then led a

magnetic,^[17] acoustic,^[18] and biological^[19] sources), the self-diffusiophoresis mechanism,^[20] self-electrophoresis,^[21] and the bubble recoiling mechanism.^[22] Tubular micro/nanomotors are established based on the bubble recoiling mechanism. The thrust comes from ejection of the generated bubbles from one end, which propels the motion of the tubular micro/nanomotors in the opposite direction. The bubble recoiling mechanism can provide high propulsion power, leading to fast movement and the ability to transport heavy cargos.

The basic principle of tubular micro/nanomotors propulsion was described in 2009^[23] shortly after the invention of these novel tubular micro/nanomotors.^[24] The fuel (hydrogen peroxide solution, H_2O_2) surrounding the tubular micro/nanomotors enters their hollow structure and is catalytically decomposed by the inner platinum (Pt) layer. Then, bubbles are

generated inside the tube and propelled out through the larger end of the microtube. The ejection of bubbles provides a jet force, which propels the forward motion of the tubular micro/nanomotors. **Figure 2a** illustrates the process of generating bubbles inside a tubular micro/nanomotor. As demonstrated here, the H_2O_2 solution fills in the microtube (Figure 2a-i), and then the O_2 bubbles produced by the reaction on the inner surface (Figure 2a-ii) nucleate and move to the larger end of the tube (Figure 2a-iii). Finally, an O_2 bubble detaches from the tubular micro/nanomotor and is released, as shown in Figure 2a-iv. The bubbles tend to move toward the larger end due to the capillary force created by the geometric asymmetry of the tubular structure.^[23–25]

To better understand the propulsion mechanism of bubble-propelled tubular micro/nanomotors, the motion behaviors of bacteria swimming at the microscale need to be analyzed. Basically, as demonstrated in Figure 1, the motion of peritrichous bacterium is driven by the rotation of their flagella.^[26] Each flagellar filament is connected to a hook that is encircled by a ring embedded in the cytoplasmic membrane of the bacterium.^[27] Sophisticated biochemical reactions inside the bacterium cause the ring to rotate in a specific direction; hence, the helical flagellar filament rotates with the ring through its bond to the hook, producing a screw-like motion. Each rotation of the helical flagellar filament generates an asymmetric configuration deformation, which allows the bacterium to move at low Reynolds numbers. By contrast, there is a mutant of *Salmonella* that has straight

flagellar filaments,^[28] and although the flagellar filaments can rotate, this mutant is stationary because the configuration does not change with the rotation of the filaments. Tubular micro/nanomotors have similar dimensions as peritrichous bacteria and an analogous hydrodynamic performance in which asymmetric configuration deformation is required for motion at low Reynolds numbers.

When regarding the tubular micro/nanomotor and a single bubble together as a system, the motion of the tubular micro/nanomotor is attributed to the asymmetric geometry deformation that occurs as the bubble grows on one side of the tube. As illustrated in Figure 2b, Li et al.^[29] presented a model to illustrate the deformation process in a micromotor-bubble system. F_{jet} and F_{bubble} denote the drag forces acting on the micro/nanomotor and the bubble, respectively. A single deformation cycle begins with stage 1, in which a bubble migrates to the end of the micromotor at a certain speed, and ends with stage 4, where the bubble detaches from the micromotor and the speed decreases to zero under the drag force. Then, another bubble is produced, and the whole deformation process becomes an asymmetric cycle. With a high frequency of bubble ejection, the discrete steps merge to generate continuous motion.

From the increased attention on tubular micro/nanomotors, several models have been built to quantitatively analyze their motion dynamics. Researchers have developed a simplified model for calculating the average micromotor speed that fits well with the experimental results.^[29] In this calculation,

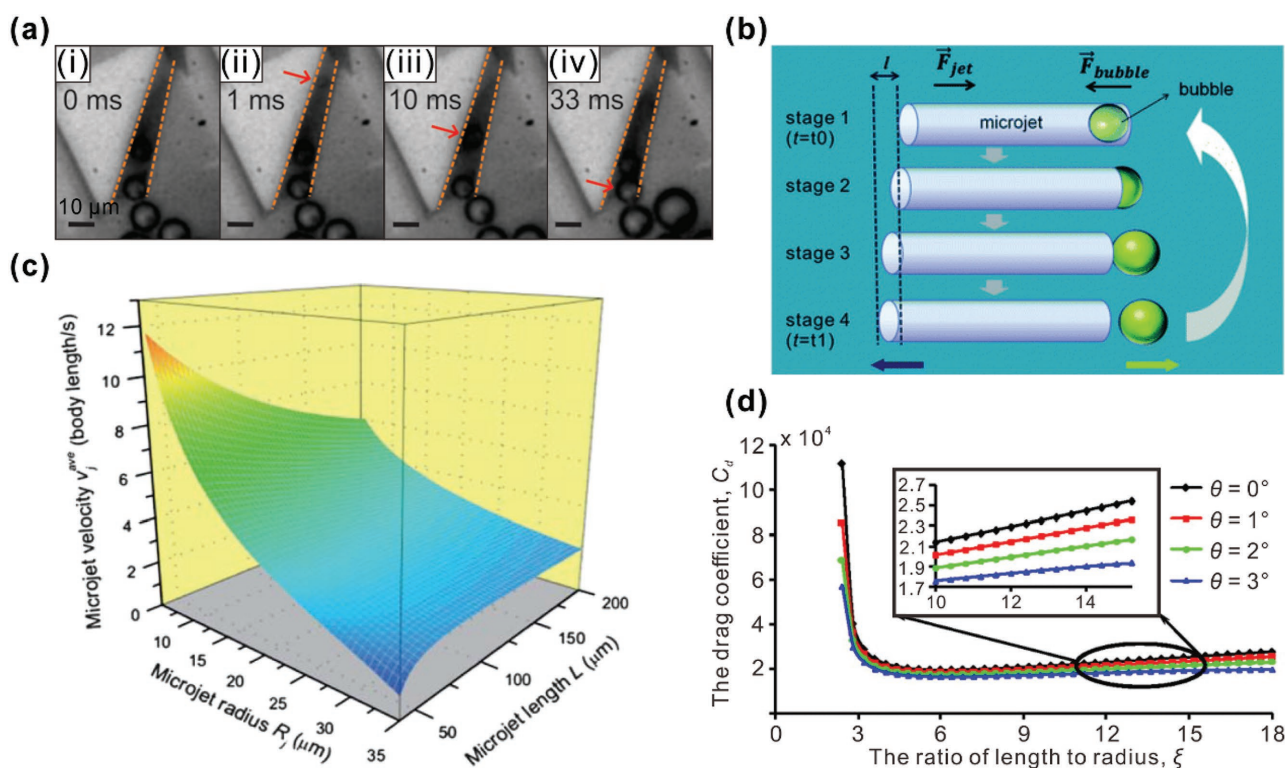


Figure 2. Propulsion mechanism of tubular micro/nanomotors. a) Bubble generation inside a tubular micro/nanomotor. Adapted with permission.^[25] Copyright 2013, IEEE. b) Scheme depicting the deformation process in the tubular micro/nanomotor-bubble system in one cycle of movement. c) Average velocity v_i^{ave} as a function of the radius R_j and length L of a microtube. b,c) Reproduced with permission.^[29] Copyright 2011, Royal Society of Chemistry. d) Drag coefficient C_d versus the ratio ξ for different semi-cone angles θ ranging from 0° to 3° for a cone frustum micro/nanomotor. Reproduced with permission.^[33] Copyright 2015, AIP Publishing LLC.

the tubular micro/nanomotor is considered to be a cylinder rolled from a rectangular nanomembrane, and the cylinder has a length L and a width $2\pi R_j$, where L and R_j are the length and radius of the cylindrical structure, respectively. The model was presented as follows

$$v_j^{\text{ave}} = \frac{9nC_{\text{H}_2\text{O}_2}R_jL}{3R_b^2 + LR_b / \left(\ln \left(\frac{2L}{R_j} \right) - 0.72 \right)} \quad (1)$$

where n is a rate constant related to the production of oxygen and can be determined from experiments, and v_j^{ave} , $C_{\text{H}_2\text{O}_2}$, and R_b are the average speed of the tubular micro/nanomotor, the concentration of H_2O_2 in solution, and the radius of the oxygen bubble, respectively. According to this equation and the corresponding calculation results shown in Figure 2c, the average speed of a micro/nanomotor is dependent not only on the concentration of the chemical fuel (H_2O_2) but also on its geometric configuration. Further derivation of the equation reveals that there is a maximum speed based on the body length per second (bl s^{-1}), and this phenomenon should be considered in regard to the applications of micro/nanomotors.

Most models, including the one described above, can only calculate the dynamic parameters of cylindrical^[30] and conical micro/nanomotors,^[25,31] but there are tubular micro/nanomotors with other geometries, such as a double cone.^[32] Thus, Li et al.^[31] provided a unified model for calculating the drag force and drag coefficient of general tubular micro/nanomotors. In this model, the tubular micro/nanomotor is considered to be immobile, and the surrounding fluid moves translationally with a constant speed. The unified drag coefficient, C_d , is introduced as follows

$$C_d = \frac{4\xi^2/Re}{(\ln\xi + \alpha)} \quad (2)$$

where $\xi = L/R_{\text{max}}$ and $\xi' = L/R_m$. R_{max} and R_m are the radius of the larger end and the cross-sectional radius of the micro/nanomachine, respectively.

In the equation for C_d , Re is the Reynolds number, and α varies for different shapes. For instance, for a cylindrical micro/nanomotor, $\alpha = -0.80685$, and for a conical tubular micro/nanomotor, α is defined by the equation

$$\alpha = -\frac{1}{2} + \ln 2 - \frac{2-\xi \tan\theta}{2\xi \tan\theta} \left[\frac{2}{2-\xi \tan\theta} \ln \left(\frac{2}{2-\xi \tan\theta} \right) - \frac{2-\xi \tan\theta}{2-\xi \tan\theta} \ln \left(\frac{2-2\xi \tan\theta}{2-\xi \tan\theta} \right) \right] \quad (3)$$

For a double-conical tubular micro/nanomotor, α is defined by another equation

$$\alpha = -\frac{1}{2} + \ln 2 - \frac{2-\xi \tan\theta}{\xi \tan\theta} \cdot \frac{2}{2-\xi \tan\theta} \ln \left(\frac{2}{2-\xi \tan\theta} \right) \quad (4)$$

where θ is the semi-cone angle of the conical structure. Figure 2d presents C_d as a function of ξ for different θ values.

C_d decreases substantially with increasing ξ from 0 to 3 and slowly increases when ξ is larger than 6. We can learn from the inset in Figure 2d that C_d is smaller when θ is larger, which means that the drag force acting on the tubular micro/nanomotor is smaller. If the tubular micro/nanomotor moves at a constant speed, the drag force and the jet force provided by the ejection of bubbles are balanced.^[25] Therefore, the jet force is also strongly related to the geometry of the tubular micro/nanomotor. To design micro/nanomotors with a higher jet force and hence a higher speed, θ should be increased. However, θ should be reduced since the ratio of the length to the radius, ξ , is usually over 6 in the fabrication of micro/nanomotors.^[33]

3. Fabrication Methodology versus Motion Control

3.1. Fabrication Methodology

As mentioned above, tubular micro/nanomotors utilize a specific chemical reaction to generate bubbles inside the tube. For most situations, the chemical reaction should occur only inside the tube to generate substantial power with high efficiency. Therefore, the fabrication of micro/nanotubes with asymmetric inner and outer surfaces is needed so that only the inner surface reacts to produce thrust. In the development of tubular micro/nanomotors, two main approaches are available for constructing asymmetric micro/nanotubes with multilayered walls: rolled-up nanotechnology and template-assisted electrodeposition.

3.1.1. Rolled-Up Nanotechnology

Rolled-up nanotechnology is a fabrication method that takes advantage of strain engineering, which has been widely applied in the manufacturing of 3D tubular micro/nanostructures.^[34] The basic concept of rolled-up nanotechnology is to release a prestrained nanomembrane by etching a sacrificial layer. This method was developed more than a decade ago, where InAs/GaAs bilayer nanomembranes were rolled into micro/nanotubes by etching the AlAs underneath layer.^[35] Then, in 2008, a general rolled-up nanotechnology was reported^[24] and has become a common method for fabricating tubular micro/nanomotors due to its versatility both in the pattern design and materials available.^[36] In this self-rolled fabrication method, a photoresist layer patterned by photolithography acts as the sacrificial layer. Then, materials with an internal strain gradient are deposited on the patterned photoresist through physical vapor deposition (PVD) or chemical vapor deposition. In the PVD process, the glancing angle is commonly aligned to create a window through the shadow effect so that no material is deposited on the obscured substrate. This window serves as an etching front for the directional removal of the sacrificial layer by an etching solution. After selective etching using acetone, the prestrained nanomembranes are released and rolled into tubular structures as a result of strain relaxation. A tubular micro/nanomotor consisting of Ti/Fe/Au/Ag layers was previously reported in which the Ag component served as the catalyst for decomposing H_2O_2 into oxygen and generating propulsion power from the oxygen

bubbles. The Fe layer allowed the tubular micro/nanomotor to be controlled by external magnetic fields.^[24] A similar rolled-up nanomembrane system was reported in which Pt replaced Ag as the decomposition catalyst, as shown in **Figure 3a-i**.^[23] The length of the tubular micro/nanomotor (100 μm) was determined by the pattern size (**Figure 3a-ii**), and the diameter of the tube was $\approx 5 \mu\text{m}$, as measured from the scanning electron microscopy (SEM) image shown in **Figure 3a-iii**. The velocity of this tubular micro/nanomotor reached 2 mm s^{-1} , and different types of movement, including a straight line, rotation, and helix, were observed and could be manipulated through the external magnetic field.

Though rolled-up nanotechnology based on a photoresist sacrificial layer has become an important method for fabricating tubular micro/nanomotors, the wet etching process for removing the photoresist, which requires a supercritical point drying process, may destroy the fabricated tubular structure due to surface tension. Recently, rolled-up micromotors based on graphene oxide were developed.^[37] Without the assistance

of a sacrificial layer, researchers applied ultrasonication to release the graphene oxide films to form tubular micromotors by taking advantage of the weak bonding interface between the silicon substrate and the graphene oxide films. In this fabrication process, the suspended graphene oxide solution was first drop-casted on the substrate, followed by the deposition of Ti and Pt layers. After ultrasonication, this trilayered nanomembrane was released into solution and subsequently rolled into a tubular structure.

Furthermore, a dry-release method was recently developed in which a heating process thermally decomposes the sacrificial layer.^[38] In the dry-release fabrication process, a poly-methylmethacrylate (PMMA) layer is spin-coated on the substrate as a sacrificial layer. After deposition of an oxide structural layer as well as a metallic layer several nanometers thick, the as-fabricated sample is annealed in nitrogen to decompose the PMMA layer, causing the deposited nanomembranes to roll into tubes. At the same time, the ultrathin metallic layer nucleates into nanoparticles, thereby generating an external capillary

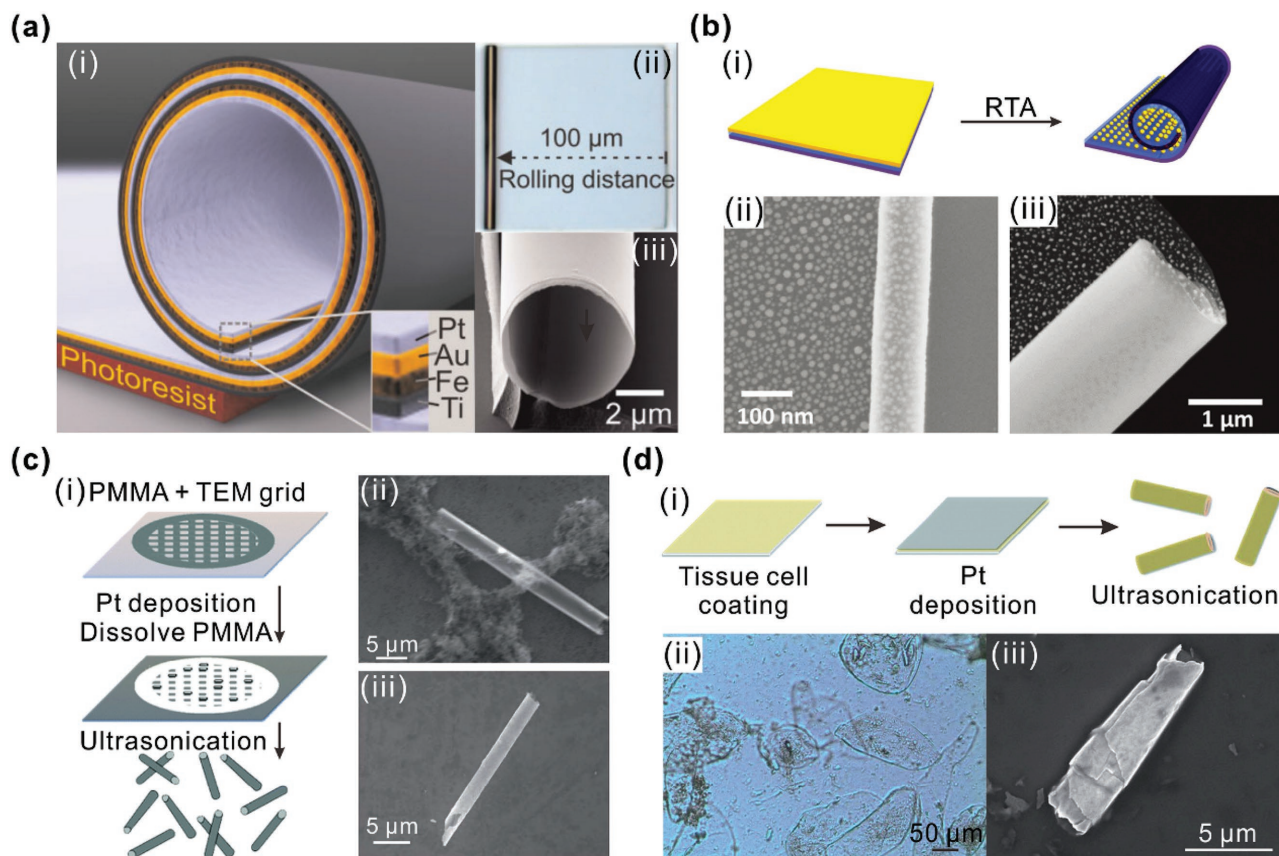


Figure 3. Tubular micro/nanomotors fabricated by the rolled-up nanotechnology. a) Self-rolling of a strain-engineered nanomembrane by selective etching of the photoresist. (i) Scheme of the rolling process, (ii) optical image, and (iii) SEM image of rolled-up tubular micro/nanomotors. Reproduced with permission.^[23] Copyright 2009, Wiley-VCH. b) Self-rolled tubular micro/nanomotors prepared by the dry-release method. (i) Scheme for rolling induced by a rapid thermal annealing (RTA) treatment. SEM images of rolled-up tubular micro/nanomotors with annealed Ag (ii) and Pt (iii) metal particles. Adapted with permission.^[38] Copyright 2013, Wiley-VCH. c) Clean-room-free rolled-up fabrication method. (i) Release of the nanomembrane by dissolving the PMMA sacrificial layer and a subsequent ultrasonication treatment. (ii) SEM image of a tubular micro/nanomotor fabricated by the clean-room-free method. (iii) SEM image of a tubular micro/nanomotor released through ultrasonication after treatment with hydrogen peroxide. Adapted with permission.^[39] Copyright 2014, Royal Society of Chemistry. d) Tissue-cell-assisted rolled-up fabrication. (i) Removal of the tissue cell coating by ultrasonication to release the Pt layer. (ii) Optical image of the tissue cell coating as a sacrificial layer. (iii) SEM image of a tubular micro/nanomotor fabricated by the tissue-cell-assisted rolling method. Adapted with permission.^[40] Copyright 2014, Royal Society of Chemistry.

force for rolling (Figure 3b-i). The tubular micro/nanomotors produced by this method had diameters as low as hundreds of nanometers, which cannot be obtained from only the internal strain gradient present in deposited nanomembranes. Furthermore, the catalytic metallic nanoparticles, such as Ag and Pt (Figure 3b-ii,iii), provided a high surface to volume ratio that accelerated the decomposition of hydrogen peroxide, resulting in a higher moving speed.^[38]

Other simple methods for preparing rolled-up micro/nanomotors have also been proposed. For example, Pumera and co-workers^[39] used a transmission electron microscope (TEM) grid to pattern the nanomembrane, allowing micro/nanomotors to be generated without requiring a clean room for photolithography. In this work, PMMA served as the sacrificial layer, which was removed by dissolution (Figure 3c-i). Pure Pt microtubes were fabricated, as shown in Figure 3c-ii. To generate these tubes, a prestressed nanomembrane was deposited on the substrate and released by H₂O₂ treatment and direct ultrasonication. Unlike the tubes discussed above, the fabricated microtubes had an irregular end (Figure 3c-iii). To rapidly prepare large quantities of tubular micro/nanomotors without requiring complex procedures, tissue cell was applied to help construct the tubular micro/nanomotors (Figure 3d-i).^[40] The tissue cells were first dispersed in water and deposited on the substrate (Figure 3d-ii), which was followed by the deposition of Pt. The layer of tissue cells was removed through ultrasonication, leaving behind a pure Pt nanomembrane that rolled into tubular micro/nanomotors (Figure 3d-iii). These two strategies provide easier fabrication methods with fewer requirements and lower cost, which may facilitate the future investigation of the rolled-up nanotechnology.

The rolled-up nanotechnology offers a convenient method for manufacturing tubular micro/nanomotors with tunable diameters and lengths. With a deeper understanding of the mechanics at the micro/nanoscale, the rolling process can be carefully tuned by altering the pattern of the sacrificial layer and the deposition parameters,^[41] leading to better control over the geometry of the tubular micro/nanomotors. In addition, the photoresist sacrificial layer permits the use of a wide range of inorganic materials, and with other sacrificial layers, the components of tubular micro/nanomotors can be extended from inorganic materials to organic materials as well as combinations of both. The versatility in the geometric design and available materials offers promising prospects for rolled-up tubular micro/nanomotors.

3.1.2. Template-Assisted Deposition and Coating

Unlike in the rolled-up nanotechnology in which 2D nanomembranes are deposited on a flat substrate and then reconstructed into 3D tubular micro/nanomotors, in the template-assisted deposition method, the materials are grown on/in templates to directly form 3D structures. Thus, the shape of the tubular micro/nanomotors can be conveniently designed by choosing a template with a specific shape. Template-assisted deposition can be divided into two classes based on the type of template: template-inside fabrication (such as wires, as shown in Figure 4a–d) and template-outside fabrication (such as porous templates, as shown in Figure 4e–h).

Materials deposited on a micro/nanowire template are given a tubular structure by selectively removing the inner wire (Figure 4a). As early as 2000, researchers used a polymer wire as the template, which was removed by thermal degradation, leaving the deposited polymer or metal as micro/nanotubes.^[42] In addition, this template-inside fabrication method was applied to generate nanotubes of GaN, a popular semiconductor material.^[43] Hexagonal ZnO nanowires were chosen as the template for the growth of single-crystal GaN. After removing the ZnO nanowires, perfect single-crystal GaN nanotubes were obtained for future applications. The first report of micro/nanotubes prepared by this method for the purpose of self-propulsion was published in 2010 and used Ag wire as the template.^[44] The wire was first etched into a conical shape by HNO₃ (Figure 4b-i). Then, a Pt/Au bilayer nanomembrane was grown on the surface of the wire by electrodeposition. After shaping and complete etching of the wire, conical tubular micro/nanomotors (Figure 4b-ii) were constructed and released, and these tubes were able to move in a solution of hydrogen peroxide.^[44]

The template-inside fabrication method could be further investigated in the preparation of graphene-based tubular micro/nanomotors. Recently, the fabrication of graphene fibers with tunable lengths and diameters by a one-step method was reported.^[45] First, a suspension of graphite oxide was injected into a glass pipeline with a diameter of hundreds of micrometers. The pipeline was then sealed and heated at 230 °C for 2 h to obtain a graphene fiber inside the pipeline. Hence, the porous graphene fiber lost its water and the diameter decreased to tens of micrometers due to capillary force. To prepare a tubular structure instead of a fiber, a Cu wire was placed in the middle of a glass pipeline as a template.^[46] The hydrothermally reduced graphite oxide aggregated around the Cu wire, and the dried graphene microtubes were released by etching the Cu wire in an FeCl₃/HCl solution (Figure 4c-i). Several Cu wires were applied together as templates to produce microtubes with multichannels (Figure 4c-ii,iii). Moreover, the outer wall could be modified with functional materials (e.g., Pt, Pd, TiO₂ nanoparticles)^[46] before etching of Cu wire. If Cu wire was covered with functional nanoparticles, these particles would be decorated into the inner wall of graphene microtubes. Therefore, graphene-based tubular micromotors were prepared successfully with Pt nanoparticles on the inner wall and ferromagnetic materials embedded in the wall, where the latter one provided magnetic control.^[46] Except that those methods for the fabrication of tubular micro/nanomotors, there were well-known tubular structures called hydrothermally grown micro/nanotubes.^[47] However, they were seldom adopted for the application in micro/nanomachines, which could be due to the difficulty of Pt coating inside the tube wall.

Nevertheless, the production of a myriad of tubular micro/nanomotors by this template-inside fabrication method through shaping of the conical wire is difficult. Thus, a template-outside electrodeposition method based on a polycarbonate membrane template containing numerous uniform double-conical micropores was developed for the fabrication of polymer/metal bilayer tubular micro/nanomotors (Figure 4d).^[48] Unlike in the previous method, the coating was grown inside the template rather than on the outside of the wire. In this method, a polyaniline (PANI) layer was first deposited along the pores of the

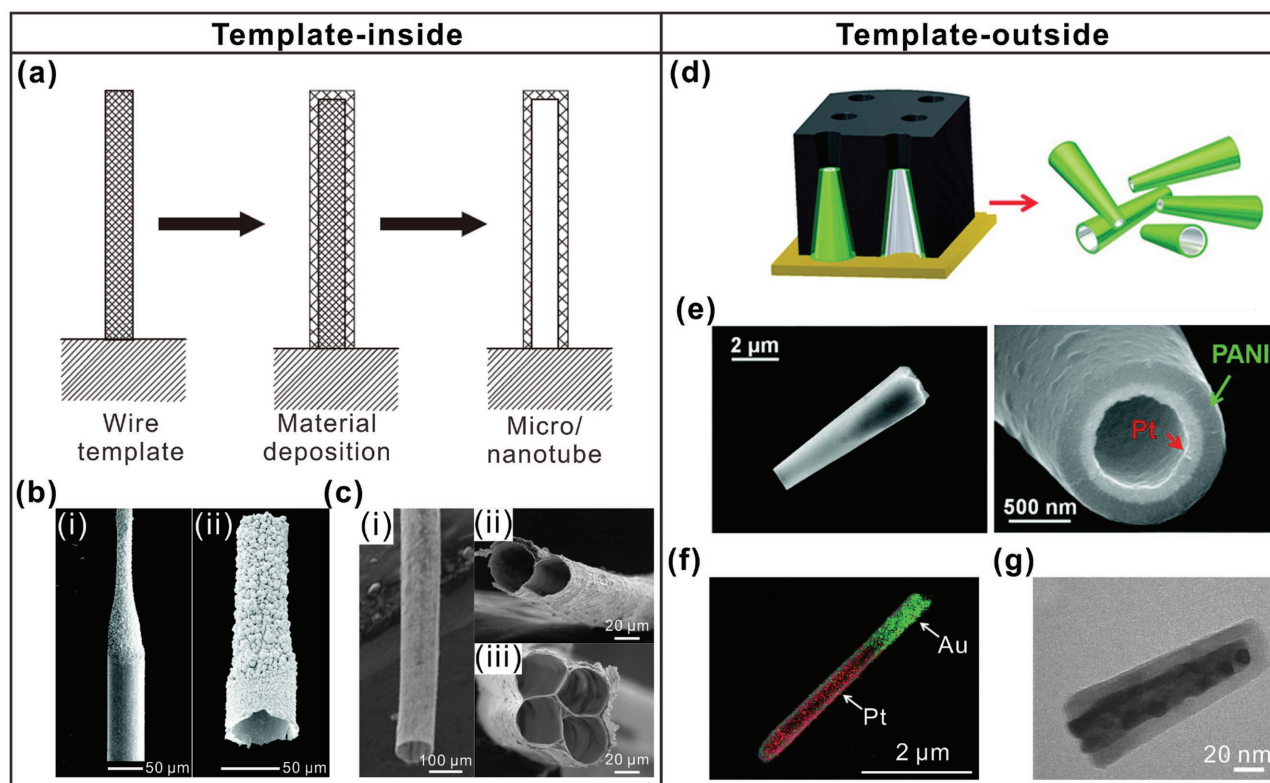


Figure 4. Tubular micro/nanomotors fabricated by template-assisted electrodeposition. a) Template-inside fabrication of micro/nanotubes via deposition on a wire. Adapted with permission.^[43] Copyright 2003, Nature Publishing Group. b) SEM images of (i) an etched Ag wire and (ii) a fabricated Pt/Au tubular micro/nanomotor. Reproduced with permission.^[44] Copyright 2010, American Chemical Society. c) SEM images of hydrothermally fabricated graphene tubular micromotors with one (i), two (ii), and four channels (iii). Reproduced with permission.^[46] Copyright 2012, American Chemical Society. d) Template-outside fabrication of micro/nanotubes with the assistance of a porous polymer template. Adapted with permission.^[48] Copyright 2011, American Chemical Society. e) SEM images of a tubular micro/nanomotor from the (ii) side view and (iii) cross view. Reproduced with permission.^[48] Copyright 2011, American Chemical Society. f) SEM/X-ray energy dispersive spectroscopy mapping (SEM/EDX) of a Pt/Au tubular nanomotor fabricated from an AAO template. Reproduced with permission.^[53] Copyright 2013, Royal Society of Chemistry. g) TEM image of a single tubular nanomotor fabricated by ALD on a copolymer template. Reproduced with permission.^[54] Copyright 2017, Wiley-VCH.

template through electrostatic and solvophobic interactions. A catalytic Pt layer was subsequently grown on the PANI layer via galvanostatic deposition. After dissolving the polymer template, PANI/Pt bilayer tubular micro/nanomotors with conical shapes were successfully prepared (Figure 4e), and these micro/nanomotors exhibited a speed of motion over 350 bl s^{-1} .

This template-assisted electrodeposition method provides an easy way to fabricate large amounts of tubular micro/nanomotors without complex fabrication requirements. As the polymer-based tubular micro/nanomotors demonstrated, this template-assisted electrodeposition method is suitable for fabricating fully inorganic tubular micro/nanomotors. For example, Cu/Pt bilayer tubular micro/nanomotors were successfully fabricated through template-assisted electrodeposition^[49] in which Cu and Pt were sequentially grown in the micropores of a polycarbonate template through two electrodeposition steps. In addition, the bimetallic tubular micro/nanomotors released after removing the template were able to move in a solution with an extremely low concentration of H_2O_2 (0.2 wt%). Moreover, the preparation of graphene/metal tubular micro/nanomotors based on the template-assisted electrodeposition method was reported in 2015.^[50] In this fabrication process, the porous polycarbonate template was first sputtered with a thin layer of Au on the

branched side for use as an electrode. Graphene oxide was then grown via a cyclic voltammetry technique and subsequently reduced by continuous cyclic voltammetry. Layers of Pt and Au were then deposited using a galvanostatic method. Finally, to release the bilayer tubes, the template was dissolved, and the Au electrode was removed by hand polishing with an alumina slurry.^[50] Tubular micro/nanomotors consisting of different carbon nanomaterials have also been developed.^[51] Furthermore, layer-by-layer (LbL) assembly through electrodeposition was proposed as an optimal technique for growing multilayer nanomembranes.^[52] The LbL method permits the growth of various materials, including polymer layers, nanoparticles, and inorganic and organic molecules. By simply immersing the porous template in solutions containing oppositely charged molecules, polymer-based tubular micro/nanomotors with catalytic metallic nanoparticles inside were prepared.

In addition to the above fabrication methods based on polymer templates, nanoporous anodic aluminum oxide (AAO) can also serve as a template for electrodeposition.^[52,53] For example, Cu was first grown as a sacrificial layer followed by the growth of Au and Pt. Finally, Au/Pt tubular micro/nanomotors were released after etching the Cu sacrificial layer in HNO_3 (Figure 4f). Recently, a copolymer template-assisted method for the synthesis

of tubular nanomotors was reported.^[54] The template was fabricated via block copolymer lithography^[55] and consisted of a porous photoresist layer covered with a 40 nm thick polymer layer. Instead of electrodeposition, atomic layer deposition (ALD) was applied to deposit TiO₂ and Pt layers several nanometers thick (Figure 4g). The resulting tubular micro/nanomotors were released from the substrate by etching the top polymer layer with a mechanical scribe.

The fabrication of tubular micro/nanomotors via the template-assisted electrodeposition method is accomplished without a clean room and complex photolithography and deposition processes. Using a porous template, this method can fabricate a large number of tubular micro/nanomotors in one procedure, and the shape of the micro/nanotubes, including the length, diameter, and symmetry, can be easily tuned by choosing templates with specifically designed micro/nanopores. On the other hand, this method sacrifices the versatility of the available materials, as only certain kinds of materials can be grown due to the limited materials available for electrodeposition and ALD. However, the desired versatility could be achieved through technological development of the templates and deposition methods.

In summary, these two methods of template-inside and template-outside functionalization, which are the main methods of fabricating tubular micro/nanomotors, have both proven their utility in the fabrication of high quality functionalized tubular micro/nanomotors on a large scale. Recently, 3D printing and writing technologies have become highly developed and can produce miniscule structures with precise control of the design down to the hundreds of nanometers, which offer great opportunities for the manufacturing of tubular mesostructures.^[56]

3.2. Motion Control

As with any motile invention, the maximum speed that tubular micro/nanomotors can achieve is of constant interest.^[57] Substantial propulsion power is generated by the bubble recoiling mechanism such that the first reported tubular micro/nanomotors reached a speed of 2 mm s⁻¹.^[23] Faster speeds suggest that the micro/nanomotors can transport more cargo and may operate in environments with a low fuel concentration and high viscosity. Thus, considerable efforts have been devoted to improving the speed through different strategies. For instance, compared to tubular structures with symmetric ends, a conical shaped micro/nanomotor tends to move faster due to the more efficient generation and ejection of bubbles.^[48] The size of the tubes also affects the speed.^[58] Since the bubbles are produced via a chemical reaction and the speed is dependent on the size and ejection frequency of the bubbles, an optimal method for enhancing the speed of the tubular micro/nanomotors is to accelerate the chemical reaction. An enlarged reaction area provides a faster rate of reaction and is easily obtained by creating a rough surface. Tubular micro/nanomotors fabricated through dry-release rolled-up nanotechnology contain a rough inner surface due to the annealing treatment.^[38] Thus, a nearly fourfold acceleration was achieved for these motors relative to the tubular micro/nanomotors with a smooth inner surface. Metal nanoparticles have also been directly grown by ALD through the island

growth mechanism (Volmer–Weber mechanism).^[59] To prepare tubular micro/nanomotors with finely structured walls and thus an increased surface area, the same research group applied an AAO sacrificial layer in the rolled-up nanotechnology.^[60] Deposition on the AAO layer generated a hierarchical nanomembrane containing nanopores. The resulting rolled-up tubular micro/nanomotors with nanopores provided an enlarged surface area and improved the reactant accessibility. The speed increased twofold to fivefold relative to that of the smooth microtubes. Similarly, graphene/Pt and graphene/Au tubular micro/nanomotors prepared by electrodeposition contained microporous Pt and Au inner layers with highly reactive properties.^[50] These micro/nanomotors exhibited ultrafast bubble propulsion, leading to moving speeds as high as 170 bl s⁻¹ and the ability to move in an environment with an extremely low fuel concentration. In addition to the aforementioned methods for accelerating tubular micro/nanomotors, many other aspects influence the speed of tubular micro/nanomotors, including the tube components,^[61] temperature,^[62] fuel concentration,^[23,48] surfactant concentration,^[63] and pH.^[64]

Both rolled-up nanotechnology and template-assisted electrodeposition have been explored as methods for miniaturizing tubular machines to the nanoscale. In 2011, the smallest man-made jet engine recorded in the Guinness Book of World Records was fabricated via the rolled-up nanotechnology.^[65] This micro/nanomotor consisted of ultrathin In_{0.33}/Ga_{0.67}/As and GaAs layers (3 nm each) perfectly grown on an AlAs sacrificial layer by molecular beam epitaxy (MBE). Benefiting from the ultralow bending stiffness caused by the thickness of the nanomembrane and the enormous strain generated by the lattice mismatch of the bilayer, this nanomembrane system rolled into tubular structures with a diameter of 600 nm. Moreover, Li et al.^[38] successfully fabricated rolled-up nanotubes with diameters of 100–200 nm (Figure 3b) by combining the internal stress with capillary force via annealing an ultrathin metal layer into nanoparticles.

Unlike the rolled-up nanotechnology, which requires the careful design of materials, a certain layer thickness, and a strain gradient for the miniaturization of tubular micro/nanomotors, template-assisted electrodeposition can easily construct nanoscale tubular structures via the selection of a template containing nanoholes. For example, electrodeposition on an AAO template produced Au/Pt tubular micro/nanomotors with lengths and diameters of 4.5–5.0 μm and 200–400 nm, respectively (Figure 4g).^[53] Furthermore, extremely small tubular micro/nanomotors with diameters of tens of nanometers were reported very recently.^[54] A template fabricated via block copolymer lithography contained pores with a length and diameter of 150 and 60 nm, respectively. Therefore, the fabricated tubular micro/nanomotors were as small as 50–60 nm in diameter and 120–150 nm in length (Figure 4h). Such extremely small tubular micro/nanomotors exhibited valid motion even though the effect of Brownian motion is very strong at that small size. Interestingly, no obvious bubbles were generated by the nanomotors, so the motion may be attributed to a self-diffusiophoretic propulsion mechanism in which the oxygen gradient led to the directional motion.^[54]

The control of the tubular micro/nanomotor motion is a vital issue for their application. Unlike the conventional methods

used to control macroscopic machines, the construction of a micro/nanoscale machine with a control circuit is nearly impossible. Instead, numerous approaches have been investigated that use external sources to influence the direction and speed of tubular micro/nanomotors.

A simple method for establishing control over the movement of tubular micro/nanomotors is to add a ferromagnetic layer of Fe, Co, and Ni. In this way, the direction of the micro/nanomotors is easily tuned by altering an external magnetic field. As early as 2009, researchers used an external magnetic field to align tubular micro/nanomotors parallel to the direction of the magnetic field and a spinning magnetic field to rotate the tubular micro/nanomotors (Figure 5a).^[23] In addition, ferromagnetic rolled-up tubular micro/nanomotors could

self-regulate and remain suspended on the surface of a liquid through the capillary force induced by the meniscus-climbing effect.^[66] Recently, 3D closed-loop magnetic control was achieved by building eight independent electromagnetic coils in 3D space.^[67] In addition, although ferromagnetic tubular micro/nanomotors commonly move in the direction parallel to the magnetic field, they can also function as a compass after a magnetizing treatment, which means that their movement toward or away from the magnet depends on the polarity.^[68]

Light is another attractive source for controlling the motion of tubular micro/nanomotors. Unlike magnetic control, which only modulates the orientation, light control primarily alters the speed. Different mechanisms are available for utilizing light irradiation to regulate the motion. For example, Solovev et al.^[69]

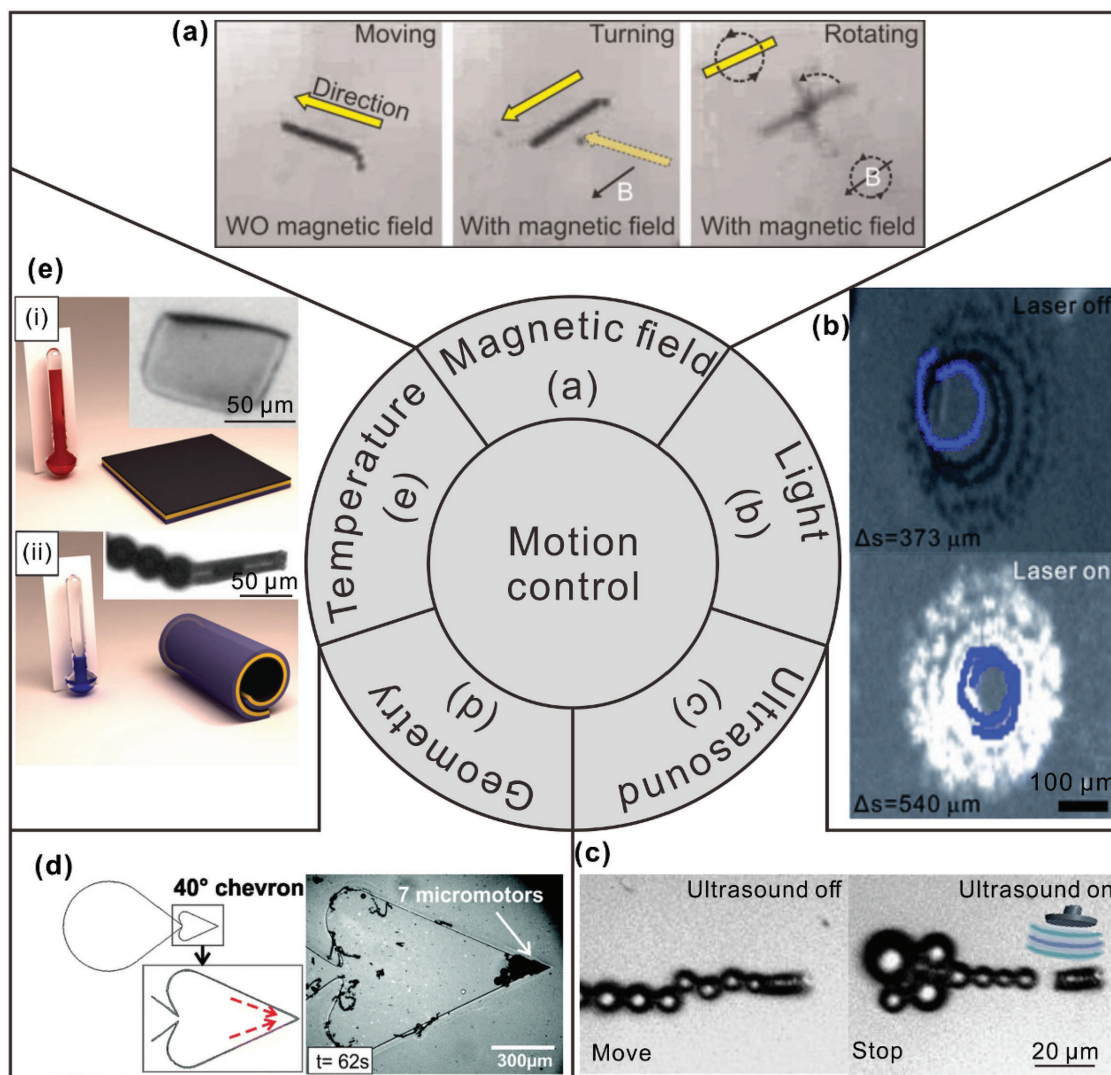


Figure 5. Control of the tubular micro/nanomotor motion. a) Magnetic control of a ferromagnetic tubular micro/nanomotor. Reproduced with permission.^[23] Copyright 2009, Wiley-VCH. b) Speed acceleration triggered by laser irradiation. Optical images of the motion of tubular micro/nanomotors without and with laser irradiation. Reproduced with permission.^[70] Copyright 2013, Royal Society of Chemistry. c) Ultrafast control of tubular micro/nanomotors with ultrasound waves. Adapted with permission.^[74] Copyright 2014, American Chemical Society. d) Geometric confinement of tubular micro/nanomotors for collection. Adapted under the terms of the Creative Commons Attribution 3.0 Unported License.^[75] Copyright 2014, the authors, published by Royal Society of Chemistry. e) Tubular micro/nanomotors based on a temperature-responsive polymer. (i) Schematic and optical image of the heat-triggered unfolding process to stop the motion. (ii) Schematic and optical image of the cooling-triggered folding process to start the motion. Adapted with permission.^[76] Copyright 2014, Wiley-VCH.

applied visible light to halt the movement of tubular micro/nanomotors on a patterned Pt substrate. The light irradiation accelerated the reaction of the fuel with the Pt substrate, thus decreasing the concentration of fuel around the tubular micro/nanomotors. At the same time, the concentration of surfactant decreased, further slowing the motion. Due to both effects, the movement of the tubular micro/nanomotors stopped under visible light irradiation and was slowly recovered in the absence of irradiation. In another method, laser irradiation was applied to accelerate the chemical reaction inside the tubular micro/nanomotors by heating the surrounding environment, which led to faster movement, and the speed could be controlled by adjusting the laser power, as shown in Figure 5b.^[70] Similarly, heat for accelerating the rate of reaction could also be provided by near-infrared irradiation.^[71] Tubular micro/nanomotors were modified with Au nanoparticles, which preferentially generated large amounts of local heat under near-infrared light irradiation due to their plasmon resonance. Such tubular micro/nanomotors exhibited “on/off” movement at a critical H₂O₂ concentration. In another system, single-component TiO₂ tubular micro/nanomotors were controlled with light by taking advantage of their photocatalytic reactivity.^[72] In this way, wireless and rapid (less than 0.2 s) control was realized because the bubble-generating reaction occurred only once the TiO₂ component was exposed to light. In another example, by adding additional photochromic molecules to the solution, the locomotion was altered by UV or visible light due to the change in the surfactant concentration caused by the reversible isomerization of the molecules.^[73]

Ultrasound energy, chip geometry, and temperature are other valid sources for manipulating or guiding tubular micro/nanomotors. Ultrasound energy was applied to modulate the motion of the motors due to its effects on the generation and evolution gas bubbles (Figure 5c).^[74] External ultrasound waves disrupt the growth of the microbubbles that form on the inner surface of the tubular micro/nanomotors. The small bubbles that are subsequently ejected do not provide sufficient power for propulsion, causing the tubular micro/nanomotors to stop moving. Thus, control with ultrasound energy provides an ultrafast (<0.1 s) and reversible way to regulate the speed. Schmidt et al.^[75] examined the effects of the chip geometry on tubular micro/nanomotor motion. The researchers designed a chip with chevron and heart shapes to trap the tubular micro/nanomotors at the apex of the chevron or confine them in the heart shape, where they could easily move but were not likely to escape (Figure 5d). In addition, a rolled-up tubular micro/nanomotor constructed in a stimuli-responsive polymer responded to temperature.^[76] The curvature of the tube changed with temperature, thus influencing the efficiency of bubble generation and leading to modulation of the speed. At a higher temperature, the tubular structure unrolled to form a flat nanomembrane (Figure 5e-i), thereby leading to static behavior, and this process could be reversed, as shown in Figure 5e-ii. Furthermore, modification of the inner wall composition by replacing the Pt catalytic layer with Pt/Cu alloy was performed to delay the movement of tubular micro/nanomotors.^[77] The micro/nanomotors were unable to move until the Cu component was consumed by a chemical reaction to expose the catalytic Pt material. The delay time was altered by changing the composition ratio of Pt/Cu and the surrounding environment.

Hence, untethered control over the motion of tubular micro/nanomotors has been realized through various methods that change their surrounding physical or chemical environment. Some methods aim to manipulate the direction, while others attempt to influence the speed. The invention of a general method for manipulating both the speed and direction of tubular micro/nanomotor motion is an important step toward the realization of smart micro/nanomotors that can respond to orders or autonomously complete designated functions.

4. Catalytic Reaction-Driven Tubular Micro/Nanomotors

Catalytic reaction-driven micro/nanomotors with a tubular geometry are one of the most popular chemically powered micro/nanomotors. Micro/nanomotors based on the bubble recoiling mechanism generate propulsion power via a chemical reaction that is accelerated by a catalyst on the inner surface of the tube. The propulsion power is provided by the surrounding solution that contains the appropriate fuel. The only requirement for the valid motion of catalytic reaction-driven tubular micro/nanomotors is the addition of the proper fuel to the surrounding environment. This peculiarity endows catalytic reaction-driven tubular micro/nanomotors with several advantages, such as prolonged navigation, reusability, and versatility. In this section, we discuss the motion driven by catalytic reactions, and Section 5 will present the noncatalytic-driven motion of tubular structures.

4.1. Catalyst versus Environment

H₂O₂ is commonly chosen as the fuel for the catalytic reaction due to its fast reaction and simple production. The decomposition of H₂O₂ produces water and oxygen, and the produced oxygen accumulates inside the tube to generate bubbles that are ultimately ejected from one end of the tube.^[23,48] In this type of tubular micro/nanomotor, a thin layer of Pt is often deposited or grown on the inner wall as a catalyst because it can dramatically improve the rate of H₂O₂ decomposition. However, since Pt is a scarce and expensive noble metal, leading to a high cost of fabrication, some substitutions have been evaluated. Similar to Pt, Ag can catalyze the decomposition of H₂O₂, although its efficiency is lower due to its oxidation.^[23] However, Ag is still a good material for replacing Pt because of its comparatively low cost. The reported tubular micro/nanomotors based on Ag reached a speed of $\approx 20 \text{ bl s}^{-1}$ in 3% H₂O₂ and were able to move in a 0.5% solution.^[78] Manganese oxide (MnO₂) is another functional catalyst and is more suitable for *in vivo* applications than Pt, which may be deactivated by small molecules such as proteins and salts.^[79] However, MnO₂ suffers from self-destruction during the catalytic reaction, and as a result, the tubular micro/nanomotors can move for approximately only 10 min. Despite this property, MnO₂ has been applied to prevent the deactivation of Pt by thiols, which are widely used to modify the Au layer in the functionalization of tubular micro/nanomotors.^[80] The MnO₂ coating on Pt prevented contact between Pt and the solution containing thiols until the tubular micro/nanomotors were

immersed in a H_2O_2 solution. In addition, considering that these inorganic catalysts may have similar effects as living organisms, the catalase enzyme was modified to provide propulsion power and improve the biocompatibility.^[81] Recently, a new catalytic reaction for propulsion was reported in which biofriendly urea was catalytically decomposed into NH_3 and CO_2 by urease located on the inner wall of the nanotube.^[82] Since no bubbles were observed during propulsion, the researchers attributed the effective movement to the internal flow created by the generated molecules. The materials and fuel of this tubular nanomotor are considered biocompatible, which may provide profound potential for future biomedical applications.

In laboratory investigations, the environments surrounding tubular micro/nanomotors are carefully designed to provide optimal conditions for propulsion. However, the practical applications of tubular micro/nanomotors occur in complex, real-world environments or bodily fluids. The presence of many particles and components in these complex matrices may hinder the motion of tubular micro/nanomotors. To investigate this hypothesis, Zhao et al.^[83] tested the motility of tubular micro/nanomotors in various real-world environments, including tap water, rain water, lake water, and sea water. The frequency of bubble ejection and motility of the catalytic reaction-driven tubular micro/nanomotors were found to be influenced by these different environments. In particular, the tubular micro/nanomotors were unable to eject bubbles and move in these liquids without a certain dilution. This lack of motility might be attributed to the high concentration of ions in the real-world environments and to other unexpected issues, which still require more exploration. To determine the suitability of catalytic reaction-driven tubular micro/nanomotors for *in vivo* applications, their motility was examined in bodily fluids, such as blood.^[84] The results of those experiments showed that both the high viscosity and high electrolyte concentration of blood hindered the locomotion of the tubular micro/nanomotors. However, an increase in the temperature from room temperature to physiological temperature dramatically accelerated the catalytic reaction, leading to valid motion in $10\times$ diluted blood.^[85] The challenge for obtaining tubular micro/nanomotors that can move in these real-world environments is to enhance their propulsion power, which should therefore be one of the future directions. In addition, upon specific functionalization, these tubular micro/nanomotors can complete several tasks, such as cargo delivery, molecule detection, and water purification, in complex environments, as described in the following section.

4.2. Cargo Collection and Delivery

The basic function of a motor, including those at the micro- and nanoscale, is to transfer selected cargos to a desired place. Solovev et al.^[86] reported the capture of cargos through magnetic force. The catalytic reaction-driven tubular micro/nanomotor in the system was fabricated by rolling of a Ti/Fe/Pt nanomembrane. Without additional modification, the tubular micro/nanomotors could catch and transport numerous particles, thereby illustrating the substantial towing force provided by the tubular micro/nanomotors based on the bubble recoiling mechanism. Furthermore, the tubular micro/nanomotors, which

floated on the solution and moved at the interface between the water and air,^[87] were able to catch floating metallic nanoplates and assemble them into regular arrays (Figure 6a). This delivery property was expanded to catch and directionally transport microparticles and cells in microfluidic channels.^[88]

The ease of modification provides access to diverse biofunctions, such as the selective capture, transport, isolation, and release of biomolecules. Kagan et al.^[89] developed a tubular micro/nanomotor fabricated via the template-assisted electrodeposition method that rapidly isolated nucleic acid targets through its surface modification. The fabricated tubular micro/nanomotors were half-coated with Au via a deposition method. Then, the tubular micro/nanomotors were modified with a binary self-assembled monolayer of a thiolated capture probe and short-chain 6-mercapto-1-hexanol. The modified tubular micro/nanomotors selectively collected the surrounding targets, including single-stranded DNA, and the collection efficiency was highly improved by the local convection induced by the ejection of bubbles. Furthermore, these tubular micro/nanomotors carrying the target DNA moved forward to escape from untreated samples, such as human serum.^[89] Thus, the biofunctionalized tubular micro/nanomotors realized the selective capture, delivery, and isolation of target DNA in a complex sample solution and transported the cargo to a clean downstream zone for further investigation. A similar strategy was also applied to rolled-up tubular micro/nanomotors.^[90] The fabricated metallic tubular micro/nanomotors were subjected to a deposition process that coated half of the tube with Au. Then, the Au surface was modified with streptavidin, which could capture biotinylated beads. In another investigation, Orozco et al.^[91] developed a molecular imprinting method for fabricating polymer-based, catalytic reaction-driven tubular micro/nanomotors with biofunctions. The molecular imprint was applied during electrodeposition of the outer poly(3,4-ethylenedioxythiophene) (PEDOT) layer so that after etching the template, the tubular micro/nanomotors were directly biofunctionalized with binding sites without additional modification. The recognition properties of the outer wall were maintained under harsh operating conditions, such as high temperature, pressure, and extreme pH.^[91] Later, researchers used both biofunctionalized tubular micro/nanomotors to capture and isolate anthrax simulant spores and unmodified tubular micro/nanomotors to mix a mildly oxidizing solution to achieve the destruction of these biothreat spores. In addition, the elimination of the spores was visually confirmed via the biofunctionalized tubular micro/nanomotors.^[92]

The strong propulsion power produced by tubular micro/nanomotors allows them to deliver not only small biomolecules, such as nucleic acids, but also large particles, such as cells. Modification of the outer Au surface of tubular micro/nanomotors with an antibody was proposed to impart the ability to selectively capture and isolate cancer cells within a designated area (Figure 6b, upper: schematic diagram and lower: captured image), and the cancer cells were shown to remain viable in a low concentration of H_2O_2 for a long period.^[93] The similar capture and isolation of other types of cells is believed to be made possible by the appropriate modification.

Although tubular micro/nanomotors with the ability to selectively capture target molecules and particles can be obtained

through proper modification, the release of these targets remains an important issue for further research on targets and the reutilization of tubular micro/nanomotors. Wu et al.^[52] developed a release mechanism in tubular micro/nanomotors that was triggered by physical stimuli. In this research, a multilayered tubular micro/nanomotor was prepared by the

template-assisted LbL method, and drug release was achieved under ultrasonic treatment by breaking the outer shell of the tubular micro/nanomotors. The researchers developed another method for realizing the light-triggered release of drugs (Figure 6c-i).^[94] In this method, the inner wall of the tubular micro/nanomotors was modified with a heat-sensitive gelatin

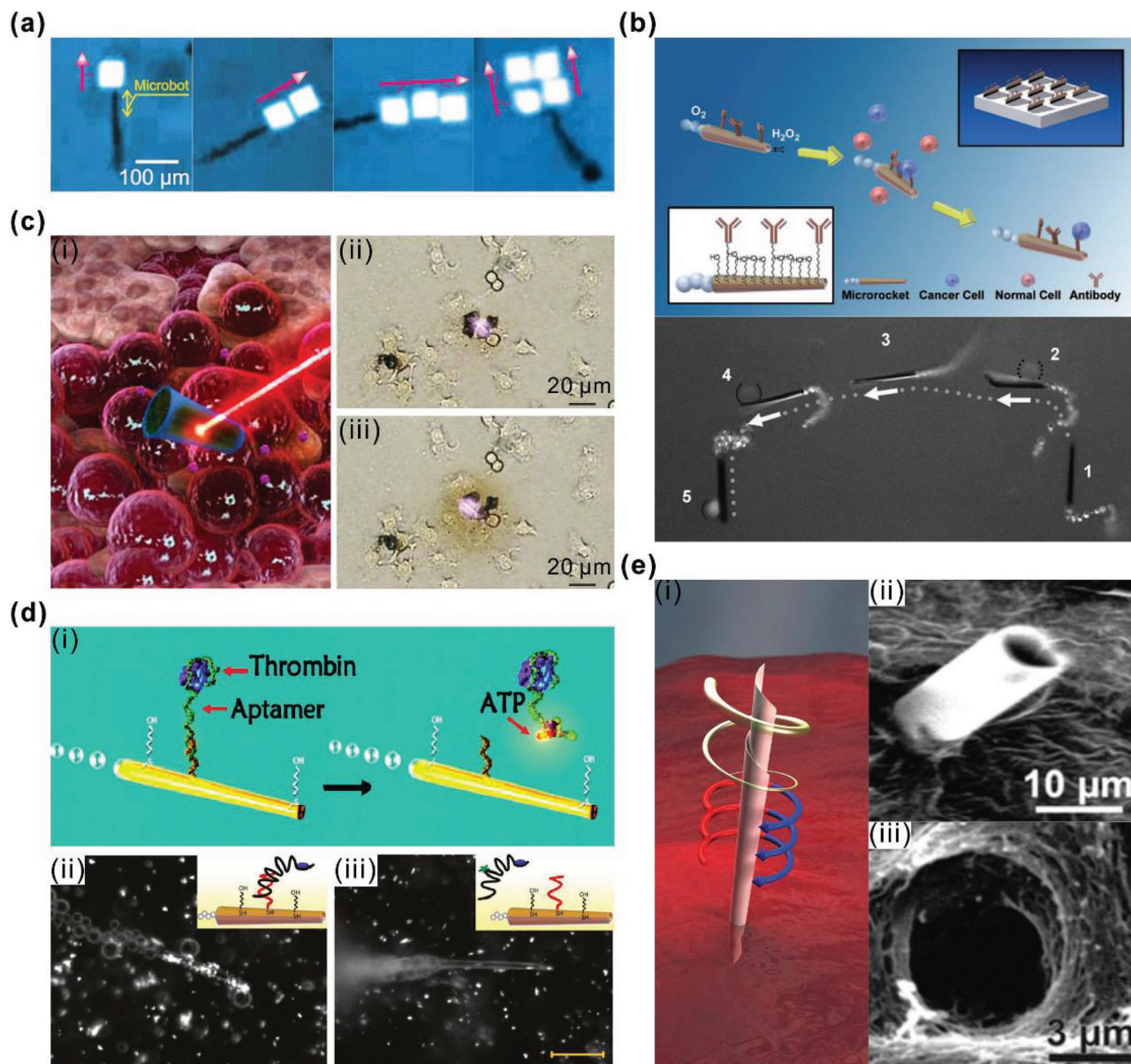


Figure 6. Cargo delivery and release achieved by tubular micro/nanomotors. a) Capture and self-assembly of metallic nanoplates through the magnetic control of tubular micro/nanomotors. Adapted with permission.^[86] Copyright 2010, Wiley-VCH. b) Biofunctionalized tubular micro/nanomotors for the selective isolation of cancer cells. (i) Scheme showing the modification of tubular micro/nanomotors with an antibody for the delivery of cancer cells. (ii) Overlay images depicting the capture and delivery processes. Reproduced with permission.^[93] Copyright 2011, Wiley-VCH. c) Drug transport and light-induced release by biodegradable tubular micro/nanomotors. (i) Scheme of drug release triggered by light. (ii) and (iii) Time-lapse images of drug release (brown solution) triggered by a near-infrared laser (purple spot). Reproduced with permission.^[94] Copyright 2014, American Chemical Society. d) Isolation and ATP-triggered unloading of proteins by aptamer-modified tubular micro/nanomotors. (i) Scheme showing protein release triggered by ATP. (ii) and (iii) Images showing the release of proteins from tubular micro/nanomotors in an environment containing ATP. Reproduced with permission.^[95] Copyright 2011, American Chemical Society. e) Nanotools for conducting micro- or nanosurgery. (i) Scheme depicting a tubular micro/nanomotor drilling into an organ. (ii) SEM image of a tubular micro/nanomotor embedded in a pig liver after drilling. (iii) SEM image of the hole drilled in the pig liver after removal of the tubular micro/nanomotor by a magnet. Adapted under the terms of the Creative Commons Attribution 3.0 Unported License.^[99] Copyright 2013, the authors, published by Royal Society of Chemistry.

hydrogel layer containing Au nanoparticles and drugs. Near-infrared light produced considerable heat around the Au nanoparticles, thus triggering a phase transition of the gelatin hydrogel and leading to rapid release of the drugs (Figure 6c-ii,iii). In addition, the tubular micro/nanomotors were made of biodegradable proteins and completely disappeared within several days upon enzymatic treatment.^[94]

Chemical and biological reactions are other powerful tools for achieving the release of the cargo. Orozco et al.^[95] demonstrated the dynamic isolation and subsequent unloading of proteins by modified tubular micro/nanomotors (Figure 6d-i). A half-coated Au layer was functionalized with mixed binding aptamers such as adenosine triphosphate (ATP) and protein-binding aptamers. The functionalized tubular micro/nanomotors moved in a solution containing the target proteins to rapidly collect the surrounding proteins (Figure 6d-ii). In addition, under the control of a magnetic field, the proteins were isolated within a separate solution. The addition of ATP to the solution triggered the release of the proteins by replacing their bonds to the functionalized tubular micro/nanomotors (Figure 6d-iii).

A release process triggered by changes in the environmental conditions was further investigated for biorelated applications. Tubular micro/nanomotors coated with a layer of Au biofunctionalized with a bioreceptor were used to selectively capture and isolate *E. coli* bacteria,^[96] which is vital for food safety and water quality related to human health. In this work, the motility of the biofunctionalized tubular micro/nanomotors was realized in a variety of real samples, including drinking water, apple juice, and seawater. After the successful isolation of *E. Coli*, their release was achieved by transferring the tubular micro/nanomotors into a low-pH glycine-based solution. After minutes of navigation, the bacteria were fully unloaded from the tubular micro/nanomotors. Moreover, a magnetic layer was incorporated in the tubular micro/nanomotors to simultaneously transport magnetic nanoparticles; thus, this system could achieve the dual transfer of bacteria and antimicrobial drugs.^[96] As another example, tubular micro/nanomotors were prepared from a poly(3-aminophenyl-boronic acid) (PAPBA)/Ni/Pt trilayer for the capture of yeast cells.^[97] The outer PAPBA layer provided strong binding to the glucose molecules and sugar components on the walls of the yeast cells. After the selective capture and transport of the yeast cells, their release was triggered by adding fructose, which binds more strongly to the boronic acid ligand, thereby taking the place of the bound sugar components on the yeast cells to liberate them from the tubular micro/nanomotors.

As demonstrated above, tubular micro/nanomotors for biomedical applications can selectively capture, transport, and release biomolecules and particles that range from proteins and drugs to cells. Another advanced biomedical application is the execution of microsurgery on organs. In 2012, a self-propelled nanotool was prepared through the careful design of the tubular shape.^[98] The researchers fabricated an InGaAs/GaAs rolled-up tubular micro/nanomotor with a sharp tip by controlling the rolling direction. This tubular micro/nanomotor preferentially moved with a curved trajectory, that is, forward motion with simultaneous rotation. Therefore, the specific motion of the tubular micro/nanomotor caused it to function like a drill, and the tubular micro/nanomotor was capable of

drilling into cells, such as HeLa cells.^[98] However, this precise control over the rolling method requires highly controlled deposition using expensive molecular beam deposition (MBE) and H₂O₂ as fuel, which may not be suitable for the surgical environment. Therefore, a Ti/Cr/Fe trilayer rolled-up tubular micro/nanomotor was later fabricated via e-beam deposition and selective etching of the sacrificial photoresist,^[99] which was patterned with a trapezoidal shape so that the trilayer membrane rolled into a tube with sharp tips on both ends. Then, a rotating magnetic field was applied to trigger the rotation of the tubular micro/nanomotor (Figure 6e-i). Interestingly, under a low frequency magnetic field, the tubular micro/nanomotor preferentially rotated its long axis parallel to the substrate. In addition, when the frequency increased to a certain threshold, the mode of tubular micro/nanomotor rotation changed such that the long axis was vertical to the substrate, thus exhibiting drilling behavior.^[99] Thus, under magnetic control, the tubular micro/nanomotor was first guided to a specific point and then drilled into an organ (Figure 6e-ii) by changing the guiding magnetic field to a high-speed rotating field. This nanodrill was subsequently removed under a strong magnetic field, leaving a hole in the organ, as shown in Figure 6e-iii. The ability to perform microsurgery with tubular micro/nanomotors provides a novel way to deliver drugs into organs and can be realized by loading drugs into the nanodrills without further treatment.

4.3. Sensing In Vitro

Benefiting from the motility of tubular micro/nanomotors, sensing by properly modified tubular micro/nanomotors represents a rapid and sensitive method for monitoring toxins and biomaterials. In addition, through clever design, the presence and concentration of target molecules can be determined in various ways. For example, the binding of molecules onto tubular micro/nanomotors can be directly observed by modifying the molecules with larger particles, which is a conventional approach in immunoassays. Gracia et al.^[100] developed catalytic reaction-driven tubular micro/nanomotors into a lab-on-chip immunoassay by functionalizing PEDOT/Ni/Pt tubular micro/nanomotors. The Ni layer provided magnetic guidance in the lab-on-chip system, allowing the tubular micro/nanomotors to swim directionally in a microchannel network. An antibody was attached to the outer surface of the tubular micro/nanomotors to capture the corresponding target protein. In addition, the protein was further modified with another antibody that was conjugated to a streptavidin-coated polystyrene particle as a tag (Figure 7a-i). The tagged protein permitted the direct visualization of the immunoreaction occurring on the surface of the tubular micro/nanomotors (Figure 7a-ii). Then, the researchers used the functionalized tubular micro/nanomotors to perform a double antibody sandwich assay with the lab-on-chip system. In this system, the tubular micro/nanomotors were first guided toward a reservoir containing different proteins, where they selectively captured the target protein. Then, the micro/nanomotors were guided to the next reservoir, where the second antibody bound to the target protein to complete the sandwich immunoassay procedure. Compared with the common double antibody sandwich assays, the

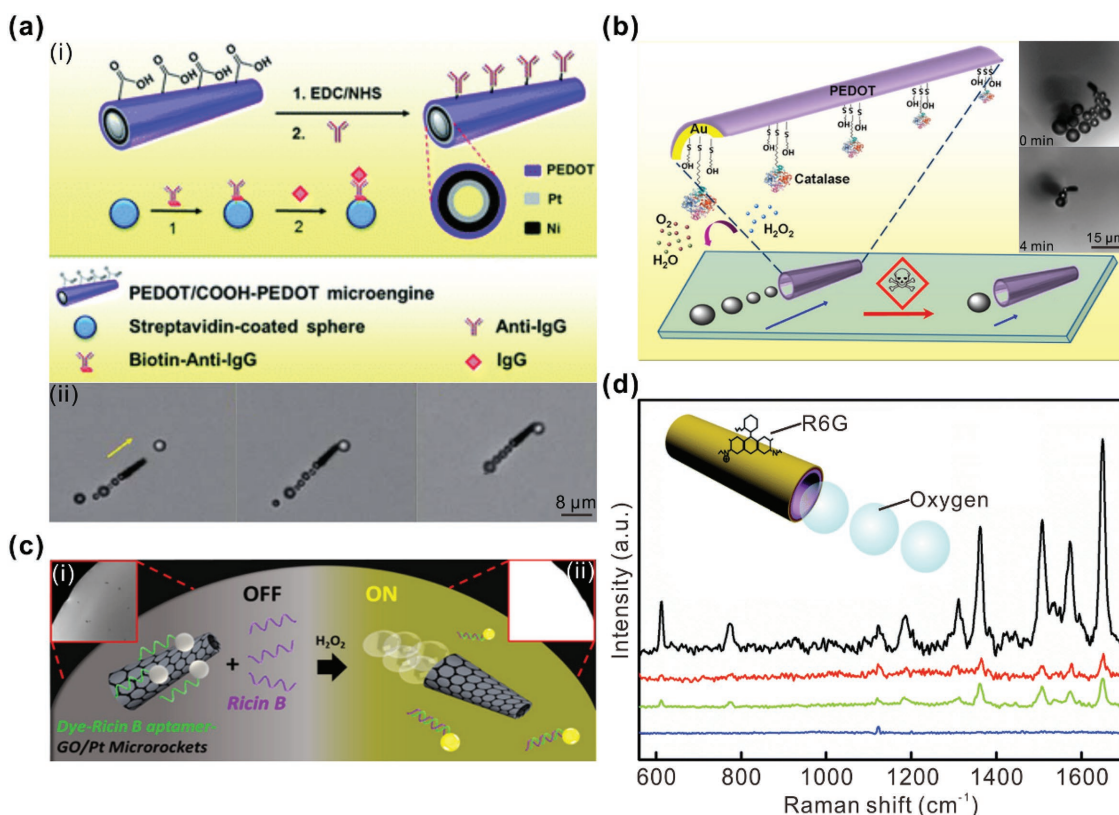


Figure 7. Rapid sensing via catalytic reaction-driven tubular micro/nanomotors. a) Lab-on-chip immunoassays by antibody-functionalized tubular micro/nanomotors. (i) Surface modification for an immunoassay observed by tagging with a second antibody. (ii) Direct observation of the immunoassay via a microparticle tag. Adapted with permission.^[100] Copyright 2013, Royal Society of Chemistry. b) Detection of toxins in water through changes in the motion of enzyme-powered tubular micro/nanomotors. The insets show that the motion is slowed in a solution containing toxins. Adapted with permission.^[103] Copyright 2012, American Chemical Society. c) Fluorescence detection of ricin by aptamer-modified tubular micro/nanomotors. The fluorescence signal changes from weak (i) to strong (ii) in the presence of ricin. Adapted under the terms of the ACS AuthorChoice License.^[108] Copyright 2016, American Chemical Society. d) Automatic collection of molecules for enhanced SERS. The Raman spectra of R6G with active tubular micro/nanomotors (black), static tubular micro/nanomotors (red), micro/nanomotors fixed on a substrate (green) and clean substrate (blue) illustrate the enhanced SERS response for the active tubular micro/nanomotors. The inset illustrates the collection of R6G by the moving tubular micro/nanomotors. Adapted with permission.^[111] Copyright 2016, Royal Society of Chemistry.

tubular micro/nanomotor-based assay eliminated the laborious multiple washing steps and saved time. Furthermore, modification of the tubular micro/nanomotors with different antibodies allowed them to capture and distinguish different antigens through conjugation to microparticles with various shapes and sizes.^[101] A further investigation was carried out to detect cancer biomarkers in situ by immunoassay.^[102] Since the collection speed of functionalized tubular micro/nanomotors is dependent on the concentration of target cancer biomarkers in solution, the concentration could be semi-quantitatively determined by counting the number of collected microspheres and analyzing the effect of the target protein on the speed, and this method was shown to be viable in untreated serum samples.

The presence of target molecules can also be indicated by variations in the speed of the motors, as these molecules may change the surface properties of the tubular micro/nanomotors. In 2013, enzyme-based tubular micro/nanomotors were applied in tests for the presence of heavy metals and other pollutants in water (Figure 7b).^[103] The enzyme attached to the inner wall of the tubular micro/nanomotors was designed to catalyze the decomposition of H_2O_2 to provide propulsion power, thus

facilitating the motion of the tubular micro/nanomotors, which could be observed by optical microscopy, as shown in the insets of Figure 7b. When the tubular micro/nanomotors were exposed to the toxins Hg, Cu, sodium-azide pesticide, and aminotriazole herbicide, the biocatalytic activity of the enzyme was quickly and irreversibly lost, resulting in attenuation of the tubular micro/nanomotor motion. Thus, the presence of these contaminants in the surrounding water could be confirmed by monitoring the movement of the tubular micro/nanomotors. Estimation of the ecotoxicological parameters, such as the exposure concentration effect and survival time, was also used to semi-quantitatively measure the concentration of contaminants. The observation of the motion was similarly applied to the detection of a nerve agent,^[104] although the procedure detected the presence of nerve agent vapor instead of its presence in solution. In this experimental design, two droplets were placed a certain distance apart on a glass slide. One droplet contained the nerve agent, and the other contained fabricated enzyme-catalytic reaction-driven tubular micro/nanomotors that navigated by ejecting bubbles. Rapid evaporation of the nerve agent filled the surrounding air with the nerve agent

vapor, which then dissolved in the second droplet containing the tubular micro/nanomotors and hindered their motion. Therefore, the presence of nerve agent in the surrounding air could be visually determined by monitoring the motion of the tubular micro/nanomotors in the droplet.

In addition to sensing toxins, Khiem and Minteer^[105] reported a DNA biosensor based on monitoring the motion of catalytic reaction-driven tubular micro/nanomotors. Unlike the above research in which the motion was hindered by the target molecules, the tubular micro/nanomotors reported herein exhibited turn-on behavior; that is, they began to move in the presence of the target DNA. The tubular micro/nanomotors consisted of PEDOT and a Au layer modified with a DNA probe. In addition, Pt particles conjugated to another DNA probe were added to the solution. The dispersed Pt catalyst could not provide propulsion power for the tubular micro/nanomotors, and these Pt particles were bound only to a DNA probe for the target DNA, which served as a bridge to connect the Pt particles and the tubular micro/nanomotors through the two DNA probes. Thus, the effective conjugation of Pt was able to degrade H₂O₂ inside the tube and propel the tubular micro/nanomotors. In this way, the presence of the target DNA was confirmed by monitoring the movement of the tubular micro/nanomotors. This biosensing method provided a detection limit as low as 1 pmol.^[105] Because this sandwich identification assay is complex and expensive, DNA biosensors were subsequently fabricated based on catalase-modified tubular micro/nanomotors.^[106] Through the same principle, the tubular micro/nanomotors were modified with DNA probes conjugated to nontarget DNA molecules that were further modified with catalase. Upon interaction between the target DNA and the tubular micro/nanomotors, the target DNA competitively bound to the DNA probe, displacing the catalase-modified nontarget DNA and resulting in a slower motion. This change in the motion of the tubular micro/nanomotors provided a semi-quantitative way to detect the target DNA.

In the field of biosensing, fluorescence is another powerful tool for analyzing biological samples through direct observation. Jurado-Sánchez et al.^[107] combined a fluorescence signal with tubular micro/nanomotors to obtain a small chemical sensor. The outer surface of tubular micro/nanomotors was modified with CdTe quantum dots that produced a strong fluorescence signal. Such tubular micro/nanomotors was able to detect toxic Hg ions, such as Hg²⁺ and CH₃Hg⁺, because the presence of these ions in solution rapidly quenched the fluorescence signal (after 12 s of navigation).^[107] The quantum dot-modified tubular micro/nanomotors could provide rapid, quantitative detection of low Hg ion concentration since the fluorescence intensity was linearly dependent on the Hg concentration up to 1 mg L⁻¹.^[107] The fluorescence of functionalized tubular micro/nanomotors was also applied in the detection of ricin, a deadly poison (Figure 7c).^[108] Reduced graphene oxide/Pt bilayer tubular micro/nanomotors containing large amounts of active sites for binding a ricin aptamer on the reduced graphene oxide surface were fabricated. The conjugated aptamers were modified with a fluorescent dye, but no fluorescence signal was observed due to the effective fluorescence quenching capability of graphene (Figure 7c-i).^[108] The detection of ricin was achieved based on the preferred conjugation of ricin to the aptamer.

The ricin in solution was rapidly collected by the moving tubular micro/nanomotors, thereby displacing the dye-labeled aptamer from the graphene surface. Rapid recovery of the fluorescence signal was therefore observed (Figure 7c-ii), leading to effective detection by changing the signal from “off” to “on”. The recovered fluorescent intensity increased linearly with increasing ricin concentration in the range from 100 pg mL⁻¹ to 10 µg mL⁻¹, providing the ability to quantitatively detect ricin in diverse biodefense scenarios.^[108] In another work, a sensor based on the fluorescence recovery of catalytic reaction-driven tubular micro/nanomotors was proposed with other carbon materials.^[109] The outer layer consisted of multiwalled carbon nanotubes or carbon black and provided a high fluorescence intensity and excellent adsorption of dyes such as rhodamine 6G (R6G). When R6G rapidly adsorbed on the carbon allotrope surface, the fluorescence signal of the tubular micro/nanomotor was quenched, which facilitated the successful detection of dyes. Consequently, in the presence of dopamine, competitive adsorption led to the desorption of R6G, resulting in the recovery of fluorescence.

In addition, without any functionalization, the stirring effect and collection properties caused by the locomotion of tubular micro/nanomotors can shorten the detection time and increase the signal intensity. For example, the motion of tubular micro/nanomotors accelerated the detection of proteins in a microarray-based immunoassay.^[110] The motion of the catalytic reaction-driven tubular micro/nanomotors created a localized vortex that transported the target molecules to the outer surface, which was functionalized with immobilized antibodies. The fluorescent intensity of the moving tubular micro/nanomotors was ≈3.5-fold higher than that of the static ones, proving the faster collection of the target protein on the detection surface. In another study, catalytic reaction-driven tubular micro/nanomotors were combined with surface-enhanced Raman scattering (SERS) to achieve more sensitive detection (Figure 7d).^[111] Tubular micro/nanomotors were fabricated through the self-rolling of Au/SiO₂/Ti/Ag multilayer nanomembranes. The outer Au layer provided outstanding SERS properties. The tubular micro/nanomotor was first moved through a solution containing target molecules such as R6G. Then, after evaporation of the water, the R6G molecules were collected around the tubular micro/nanomotor, leading to a fivefold enhancement in the Raman spectrum intensity relative to that of the immobilized tubular micro/nanomotors.

This section introduced the sensitive detection of target molecules based on tubular micro/nanomotors. When large particles are conjugated to the target, the collection process by the motile tubular micro/nanomotors can be directly observed via optical microscopy. For molecules without tags, the sensing behavior of the tubular micro/nanomotors is derived from monitoring changes in the motion (e.g., speed). Furthermore, with the assistance of fluorescence, the rapid quantitative analysis of the concentration of a molecule can be realized based on the fluorescence signal of the tubular micro/nanomotors. In addition, by combining the fast collection behavior of tubular micro/nanomotors with SERS, we can detect extremely low concentrations of the target. These tubular micro/nanomotors rapidly collect the surrounding targets during navigation, thus gathering the target molecules together to obtain ultrahigh sensitivity.^[111]

4.4. Environmental Decontamination

Environmental pollution from the increasing frequency of anthropogenic activities causes nonnegligible issues in modern society. With the development of nanotechnology, nanomaterials exhibit outstanding abilities to adsorb and degrade pollutants, such as heavy metals and organics.^[112] As discussed above, functionalized tubular micro/nanomotors can rapidly capture and collect surrounding molecules and particles while moving in solution. Applying this strategy to the field of environmental decontamination could provide a method for the rapid purification of contaminated water. The remediation of water consists of two methods: adsorption/absorption of pollutants and chemical degradation of contaminants.

Guix et al.^[113] demonstrated the first example of environmental remediation based on the rapid sorption capability of tubular micro/nanomotors. Fabricated Au/Ni/PEDOT/Pt tubular micro/nanomotors were modified with a superhydrophobic layer by the self-assembled monolayer method. With the addition of H₂O₂ and surfactant to water contaminated with oil, the functionalized tubular micro/nanomotors moved through the polluted solution to clean it. Oil droplets in the water

strongly adhered to the superhydrophobic layer, and the high propulsion power of the tubular micro/nanomotors allowed them to drag several microscopic oil droplets against the viscous force. Under the guidance of a magnetic field, the collected oil pollutant was transported to a separate area to achieve the purification of the polluted water.^[113] In another study, tubular micro/nanomotors were synthesized via LbL assembly of a poly-(styrenesulfonic acid) (PSS)/allylamine hydrochloride (PAH) multilayer followed by the electrodeposition of PEDOT and Pt inner layers.^[114] The PSS/PAH outer layer provided a large loading capability for organic pollutants, such as methyl paraoxon and R6G. The motion of the tubular micro/nanomotors enhanced the fluid dynamics, leading to more efficient absorption of organic pollutants relative to the static tubular micro/nanomotors.

Singh et al.^[115] reported the development of reusable tubular micro/nanomotors for the detoxification of nerve agents (Figure 8a). The tubular micro/nanomotors consisted of zirconia (ZrO₂) and graphene oxide, where the outer ZrO₂ layer offered unique properties, including the efficient binding of nerve agents, and the inner graphene oxide layer was coated with Pt to provide a high thrust force. The tubular micro/

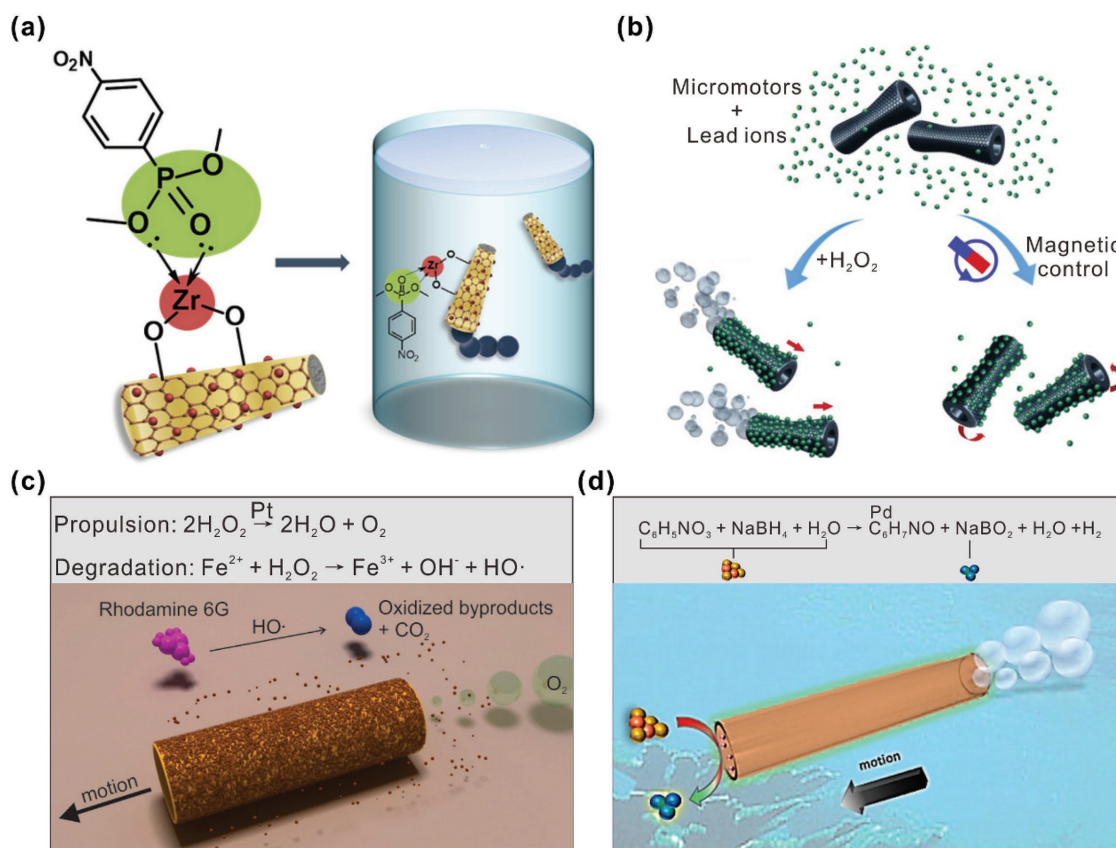


Figure 8. Environmental decontamination by catalytic reaction-driven tubular micro/nanomotors. a) Zirconia/graphene tubular micro/nanomotors for the removal of organophosphate compounds. Reproduced with permission.^[115] Copyright 2015, American Chemical Society. b) Graphene-based tubular micro/nanomotors for lead decontamination and collection. Adapted under the terms of the Creative Commons Attribution (CC-BY) License.^[116] Copyright 2016, the authors, published by American Chemical Society. c) Organic remediation by tubular micro/nanomotors based on the Fenton reaction. Adapted under the terms of the ACS AuthorChoice License.^[117] Copyright 2013, American Chemical Society. d) Remediation of 4-nitrophenol by catalytic reaction-driven tubular micro/nanomotors without the addition of fuel. Adapted with permission.^[121] Copyright 2015, American Chemical Society.

nanomotors demonstrated the highly efficient removal of the nerve agent, while the static ones or those without the outer ZrO₂ layer showed negligible adsorption. Furthermore, the nerve agent could be desorbed from the tubular micro/nanomotors through a NaOH treatment, and the recovered tubular micro/nanomotors were separated from the toxin with a magnet. Purification was also demonstrated with reusable tubular micro/nanomotors based on graphene oxide.^[116] The graphene oxide/Ni/Pt multilayer tubular micro/nanomotors were proposed to capture, transfer, and remove heavy metals, where Pb served as an example. The graphene oxide layer was able to absorb heavy metal ions in water. The catalytic reaction-driven tubular micro/nanomotors moved for a long time and absorbed most of the heavy metals (Figure 8b). Then, the functionalized tubular micro/nanomotors delivered the heavy metals to another chamber under the guidance of a magnetic field. Desorption of the heavy metals for reuse of the tubular micro/nanomotors was accomplished through an acid treatment.

The above studies achieved environmental decontamination by the absorption and adsorption of toxins. For organic pollutants, another useful remediation approach is degradation via chemical reactions. Soler et al.^[117] demonstrated the ability of bimetallic tubular micro/nanomotors without further functionalization to clean polluted water through a Fenton-like oxidation process (Figure 8c). The catalytic reaction-driven tubular micro/nanomotors were fabricated via self-rolling of Fe/Pt nanomembranes. In the presence of H₂O₂ in an acidic environment, the outer Fe layer slowly dissolved and released Fe²⁺ ions, which then reacted with H₂O₂ through a Fenton reaction in a catalytic cycle with the following two steps



The hydroxyl radical (HO[•]) generated in this reaction is a powerful oxidant that is capable of degrading organic contaminations. The degradation efficiency of the tubular micro/nanomotors was ≈12 times higher than that of immobilized Fe microtubes due to the enhanced mixing of the liquid that resulted from bubble generation and fluid flow. In addition, these Fe/Pt tubular micro/nanomotors were reusable after their collection with a magnet and could be used for several cycles with a high degradation efficiency, and they still functioned after being stored for several weeks.^[118] H₂O₂ itself is a clean reagent for efficiently decomposing chemical toxins through the generation of OOH⁻ nucleophiles. However, conventionally, decontamination systems based on H₂O₂ require a high concentration to maintain prolonged operation. Considering that the tubular micro/nanomotors are propelled by H₂O₂, the resulting self-mixing effect can accelerate the degradation efficiency of H₂O₂. PEDOT/Pt tubular micro/nanomotors without further functionalization were applied to the degradation of organophosphate nerve agents,^[119] and as much as 96.1% of the available methyl paraoxon was degraded within 20 min in the presence of tubular micro/nanomotors, whereas a negligible change in the signal was observed without tubular micro/nanomotors.

Uygun et al.^[120] applied functionalized tubular micro/nanomotors in another environmental area—carbon dioxide (CO₂) sequestration, which is important for slowing global warming. The surface of the tubular micro/nanomotors was modified with carbonic anhydrase (CA). When dissolved in water, CO₂ is hydrated and ionized to CO₃²⁻. The CA attached on the surface of tubular micro/nanomotors performed excellent CO₂ capture by catalyzing the hydration process. The mixing of the functionalized tubular micro/nanomotors substantially enhanced the sequestration efficiency such that 9.2- and 11.5-fold enhancements were obtained relative to free CA molecules and immobilized tubular micro/nanomotors with CA, respectively. Furthermore, the biofunctionalized tubular micro/nanomotors maintained their catalytic activities after storage for 30 d.^[120] Another strategy for achieving the generation of propulsion power and the remediation of polluted water was developed based on a one-step catalytic chemical reaction (Figure 8d).^[121] In this research, tubular micro/nanomotors were modified with Pd particles, which can catalyze the decomposition of the pollutant 4-nitrophenol in the presence of NaBH₄. This degradation reaction generates hydrogen bubbles, thereby simultaneously providing propulsion power. Therefore, the tubular micro/nanomotors did not require H₂O₂ fuel and surfactant. The degradation speed of this system was ≈10 times faster than that of static Pd particles.

Furthermore, highly efficient photocatalytic degradation was obtained by combining TiO₂ tubular micro/nanomotors with Pt and Pd layers.^[122] Modification with these noble metals allowed the tubular micro/nanomotors to rapidly degrade organic pollutants, such as rhodamine B, methyl orange, and methylene blue, under visible light and natural sunlight. In another demonstration, semiconductor quantum dots were attached to the outer surface of tubular micro/nanomotors during template-assisted electrodeposition.^[123] PANI containing Cd²⁺ was electrodeposited first, and the template was then immersed in a Na₂S solution to assemble CdS quantum dots on the PANI layer. The CdS quantum dot-modified PANI/Pt tubular micro/nanomotors exhibited outstanding photocatalytic degradation of bisphenol A, with complete degradation of the pollutant occurring within 10 min. Moreover, when ZnS quantum dots were introduced on the surface of the tubular micro/nanomotors, heavy metal ions (i.e., Hg ions) dynamically exchanged with Zn²⁺, leading to the efficient absorption of heavy metal ions on the surface of the tubular micro/nanomotors.

Currently, catalytic reaction-driven tubular micro/nanomotors are mainly based on the catalytic decomposition of H₂O₂. The rapid generation of oxygen bubbles allows the tubular micro/nanomotors to navigate in complex and real environments. This high thrust also provides the ability to tow heavy cargos. In addition, easy modification of the outer surface of tubular micro/nanomotors allows them to selectively capture, transport, and release target particles. Based on the binding process, tubular micro/nanomotors can rapidly collect surrounding molecules and particles for further sensing and cleaning applications. We revealed only a small portion of the research on the functionalization of tubular micro/nanomotors as well as their inspired applications. Many more types of functionalization are waiting to be discovered and will establish new applications for tubular micro/nanomotors.

5. Noncatalytic Reaction-Driven Tubular Micro/Nanomotors

While the most popular tubular micro/nanomotors are those with catalytic properties that can decompose H_2O_2 to form oxygen bubbles, high concentrations of H_2O_2 are not suitable for in vivo applications. Thus, tubular micro/nanomotors with different chemical materials that use fuels other than H_2O_2 have also been developed. Furthermore, biohybrid tubular micro/nanomotors that function independently of fuels have been demonstrated.

5.1. Chemical Reaction-Driven Tubular Micro/Nanomotors

In 2011, a tubular micro/nanomotor consisting of PANI and Zn layers was reported (Figure 9a).^[124] The inner Zn layer provided effective propulsion in strongly acidic media by generating hydrogen bubbles via the redox reaction $\text{Zn(s)} + 2\text{H}^+(\text{aq}) \rightarrow \text{Zn}^{2+}(\text{aq}) + \text{H}_2(\text{g})$. This tubular micro/nanomotor could move in different acids and perform the capture, transport, and release of cargos with an additional ferromagnetic layer. Furthermore, a Zn-based tubular micro/nanomotor with a double-conical shape was developed to more conveniently load cargos.^[32] In that study, two different particles (SiO_2 and Au nanoparticles) with different sizes (20–500 nm) were utilized as the cargo to demonstrate the ability of Zn-based tubular micro/nanomotors to transport large amounts of the various particles. Upon reaching the destination, the tubular micro/nanomotors were destroyed in the acid environment to release the cargo.

The first in vivo application was demonstrated in the acidic environment in the stomach.^[125] Zn-based tubular micro/nanomotors were operated in gastric acid and exhibited improved spreading efficiency for delivering drugs (Au particles as an example, Figure 9b-i). The binding and retention of Au particles (drugs) on the stomach wall were enhanced by the motion of the Zn-based tubular micro/nanomotors such that the drugs were able to remain in the stomach for a long period (Figure 9b-ii,iii). Furthermore, the gastric acid in the stomach dissolved the tubular micro/nanomotors to release the cargos, leaving no toxins or organisms behind. However, one weakness of this tubular micro/nanomotor is that the reaction between Zn and acid is too fast to maintain their motion for long periods, and the lifetime of the micro/nanomotors was only 20 s in strongly acid environments.^[32] Other materials were recently put forward as replacements for the Zn metal.^[126] The Fe layer that replaced Zn reacted with acid to generate hydrogen bubbles; thus, both a longer lifetime (20 min) and a higher propulsion efficiency were achieved. This research was also the first to demonstrate the self-reconfiguration of several micro/nanomotors into chain-like arrays and other structures through magnetic interactions.^[126]

Highly active metals that can react with water to produce hydrogen can potentially provide propulsion power in the absence of acid. Tubular micro/nanomotors constructed with Mg as the inner wall were capable of navigating in water, providing broad potential for in vivo applications.^[127] Interestingly, an enteric coating was applied to prevent reaction of the Mg layer until the enteric polymer dissolved in the intestinal fluid.^[127] Therefore, the tubular micro/nanomotors moved only in the

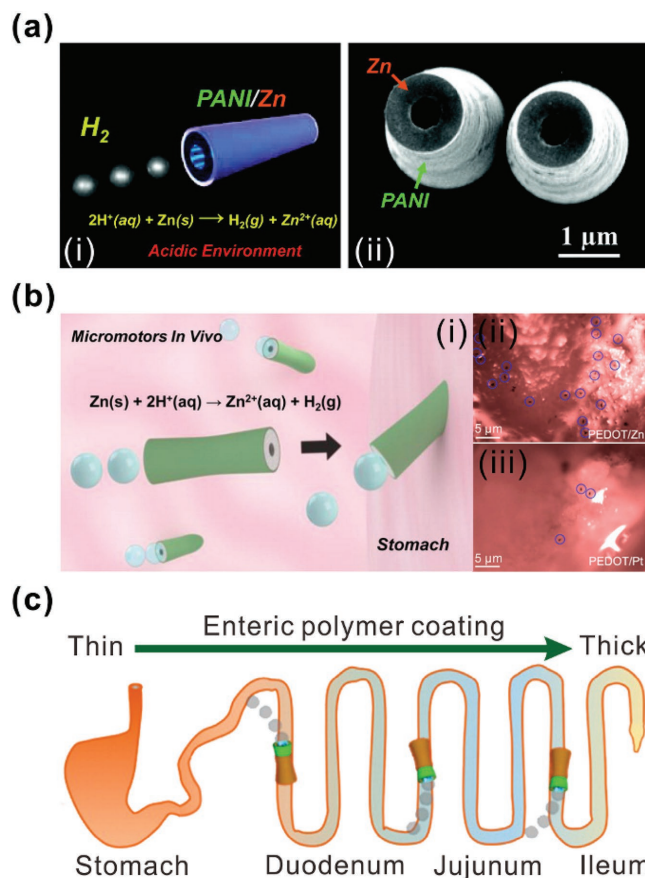


Figure 9. Chemical reaction-driven tubular micro/nanomotors for in vivo applications. a) The tubular micro/nanomotors with zinc propelled by redox reaction in acid environment. (i) Principle of propulsion. (ii) SEM image of the top view of Zn-based tubular micro/nanomotors. Reproduced with permission.^[124] Copyright 2011, American Chemical Society. b) Zn-based tubular micro/nanomotors moving inside the stomach. (i) Scheme of the micro/nanomotors motion prolonging the retention of drug. (ii) The counted tubular micro/nanomotors in stomach after 2 h compared with (iii) immobilized tubular micro/nanomotors. Adapted under the terms of the ACS AuthorChoice License.^[125] Copyright 2014, American Chemical Society. c) Controlled release of tubular micro/nanomotors in the gastrointestinal tract. The localization and retention of tubular micro/nanomotors in stomach and gastrointestinal tract are determined by the thickness of polymer coating. Adapted with permission.^[127] Copyright 2016, American Chemical Society.

gastrointestinal tract where the Mg layer was exposed, and the position of release within the gastrointestinal tract was altered by changing the coating thickness. As demonstrated in Figure 9c, a thinner coating of the enteric polymer allowed the micro/nanomotors to locally release the drug close to the stomach, while a thicker coating allowed them to reach the ileum. Through this approach, like a capsule, the drugs loaded in the tubular micro/nanomotors were released at precise locations, and faster spreading was also achieved due to the motility of the micro/nanomotors.

5.2. Biohybrid Tubular Micro/Nanomotors

Rather than searching for proper chemical reactions to provide the propulsion power needed for tubular micro/nanomotors,

nature has already provided large amounts of motile cells and microorganisms that can be incorporated in tubular micro/nanomotors. In recent years, Magdanz et al.^[128] have devoted considerable effort to developing tubular micro/nanomotors combined with spermatozoa (Figure 10a-i). In 2013, the first tubular micro/nanomotor driven by captured spermatozoa was reported.^[19a] The rolled-up microtube consisted of Ti and Fe and had a diameter of several micrometers, which was suitable for capturing spermatozoa. The direction of motion was controlled in 3D by an external magnetic field.^[129] Such guidance allowed the biohybrid tubular micro/nanomotor to move directionally in the microchannels of a lab-on-chip system. Several approaches for improving the performance of biohybrid tubular micro/nanomotors have been explored.^[130] Shorter tubular micro/nanomotors have been shown to provide faster speeds, which was attributed to the reduced confinement of

the flagellum within the walls of the microtube. Compared with the biohybrid tubular micro/nanomotors constructed by the random locomotion of spermatozoa, biofunctionalization of the inner wall provided a strong bond to the spermatozoa, resulting in a higher coupling efficiency. Furthermore, the activity of the spermatozoa could be enhanced by adding caffeine to surrounding solution to improve the speed of the biohybrid tubular micro/nanomotors.^[130]

In addition to the valid capture and transport of spermatozoa by biohybrid tubular micro/nanomotors, the release of the spermatozoa based on a temperature-sensitive polymer layer has also been achieved.^[131] At low temperature, the polymer-based nanomembrane rolled into tubular structures that were ready for coupling to spermatozoa. After the spermatozoa swam into the tubes and the biohybrid tubular micro/nanomotors moved to the desired location, the release of the spermatozoa was triggered by increasing the temperature (Figure 10a-ii). Also, higher temperatures accelerated the spermatozoa motion, allowing them to rapidly escape from the unrolled micro/nanomotors. The biohybrid tubular micro/nanomotors based on spermatozoa provide a novel treatment for infertility and may realize more biofunctions. The development of biohybrid tubular micro/nanomotors provides complete biocompatibility, which is critical for in vivo applications, and therefore, more applications can be expected in the near future.^[132]

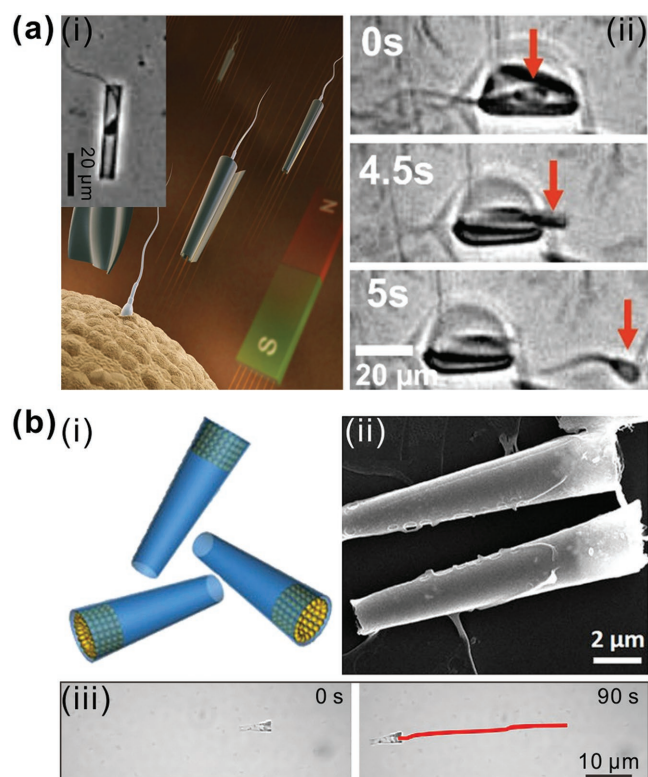


Figure 10. Biohybrid tubular micro/nanomotors and heat-propelled tubular micro/nanomotors. a) Biohybrid tubular micro/nanomotors combined with spermatozoa. (i) Illustration of the capture, transport and release of spermatozoa near an oocyte under magnetic guidance. The inset shows a spermatozoon entering a microtube. (ii) Release of spermatozoa from polymer-based tubular micro/nanomotors upon increasing the temperature. The inset of i) is adapted with permission.^[19a] Copyright 2013, Wiley-VCH. i) is adapted with permission.^[130] Copyright 2015, Wiley-VCH. ii) is reproduced with permission.^[131] Copyright 2016, Wiley-VCH. b) Tubular micro/nanomotors propelled by a thermal gradient generated via near-infrared irradiation. (i) Scheme of fabricated tubular micro/nanomotors containing Au nanoparticles on the inner wall. (ii) SEM image of the light-activated tubular micro/nanomotors. (iii) Optical images of the moving tubular micro/nanomotors propelled by a thermal gradient. Adapted under the terms of the Creative Common Attribution 4.0 International License.^[135] Copyright 2017, the Authors, published by Nature Publishing Group.

5.3. Other Types

Wang et al.^[133] developed self-propelled tubular micro/nanomotors in which the propulsion behavior was induced by the Marangoni effect as follows: the presence of surface tension gradient leads to the movement of micro-objects on the surface from an area with low surface tension to an area with high surface tension. Thus, the propulsion of these tubular micro/nanomotors required no additional fuel or modification. In addition, researchers modified tubular micro/nanomotors with enzymes for the degradation of pollutants.^[133] The enzyme was released in polluted water and transformed the pollutants into innocuous materials, while the motion of the micro/nanomotors stirred the solution and facilitated rapid degradation of the pollutant.

Moreover, a tubular micro/nanomotor activated by light was developed in which the navigation was not based on a chemical reaction. Instead, the tubular micro/nanomotor was propelled by a thermal gradient. Polymer-based tubular micro/nanomotors with Au nanoparticles inside the tube generated substantial heat under near-infrared light irradiation,^[134] and the resulting heat gradient inside the conical tube provided asymmetric thermophoretic forces for propulsion. Moreover, the deposition of Au clusters on the larger open end of cone-shaped silica tubes was demonstrated (Figure 10b-i,ii).^[135] Irradiation by near-infrared light (laser) generated a thermal gradient along the axial direction of the tube, producing a thermophoretic force that propelled the tubular micro/nanomotor (Figure 10b-iii). The speed of the tubular micro/nanomotor could be tuned by modifying the irradiation power of the near-infrared light. At a sufficiently high power, the micro/nanomotors exploded due to the ultrahigh thermal gradient produced in the silica layer.^[135]

which may provide a novel release method for biomedical applications.

From research advancements toward noncatalytic reaction-driven tubular micro/nanomotors, several *in vivo* applications have been achieved based on different power sources (e.g., Zn, Mg). However, because these systems are still far from practical application, enormous efforts are needed to meet the demands of biomedical micro/nanomotors with the further development of biocompatible catalysts and fuels. Precise control and bio-functionalization are required to guide the micro/nanomotors to a desired location inside a body and conduct biomedical functions. The marriage of materials and medical science would accelerate the development of tubular micro/nanomotors for health care and disease treatment as expected.^[136]

6. Summary and Outlook

While the development of machines has completely revolutionized industrial fabrication processes and our lifestyles, the function of machines at the micro- and nanoscale remains to be seen, as micro/nanomachines require additional research to realize their practical application. However, the tubular micro/nanomotors introduced in this review already share similarities with various macroscopic machines, such as submarines, jets, missiles, and rockets. In this review, we attempted to provide a complete picture of the tubular micro/nanomotors developed in recent decades. These tubular micro/nanomotors are commonly self-propelled through the bubble recoiling mechanism, and their velocity depends on the ejection frequency and relative size of the bubbles generated inside the tube. The methods for fabricating tubular micro/nanomotors include rolled-up nanotechnology and controllable template-assisted deposition. In the rolled-up nanotechnology, the key requirement is multilayered nanomembrane systems with strain gradient on sacrificial layers. The catalysts (typically Pt or Ag) were rolled inside tubes and functional materials coated outside. Template-assisted methods require matrixes to host materials for motors and surface coating inside/outside of adopted templates. Rolled-up method mainly relies on thin film deposition methods and planar silicon technology, while template-assisted method could be highly related to the development of porous templates and coating technology. When the 3D printing technology becomes further developed, more complex tubular micro/nanomotors for complicated motion with high power can be expected. Effective control of the speed and direction of motion is realized through both physical approaches, such as a magnetic field, light, and ultrasound energy, and chemical modification of the inner layer. A magnetic field is commonly used for motion control by simply adding ferromagnetic component as Fe, Co, and Ni. In addition, catalytic reaction-driven tubular micro/nanomotors that rely on the catalytic decomposition of H_2O_2 to generate oxygen bubbles have been developed with a variety of catalysts, such as Ag, Pt, MnO_2 , and the catalase enzyme. These systems are widely applied in the selective delivery of cargos, microdetection and sensing, and environmental remediation by taking advantage of the self-mixing effect and proper modification of the outer surface. Due to the toxicity of high H_2O_2 concentrations to organisms, noncatalytic

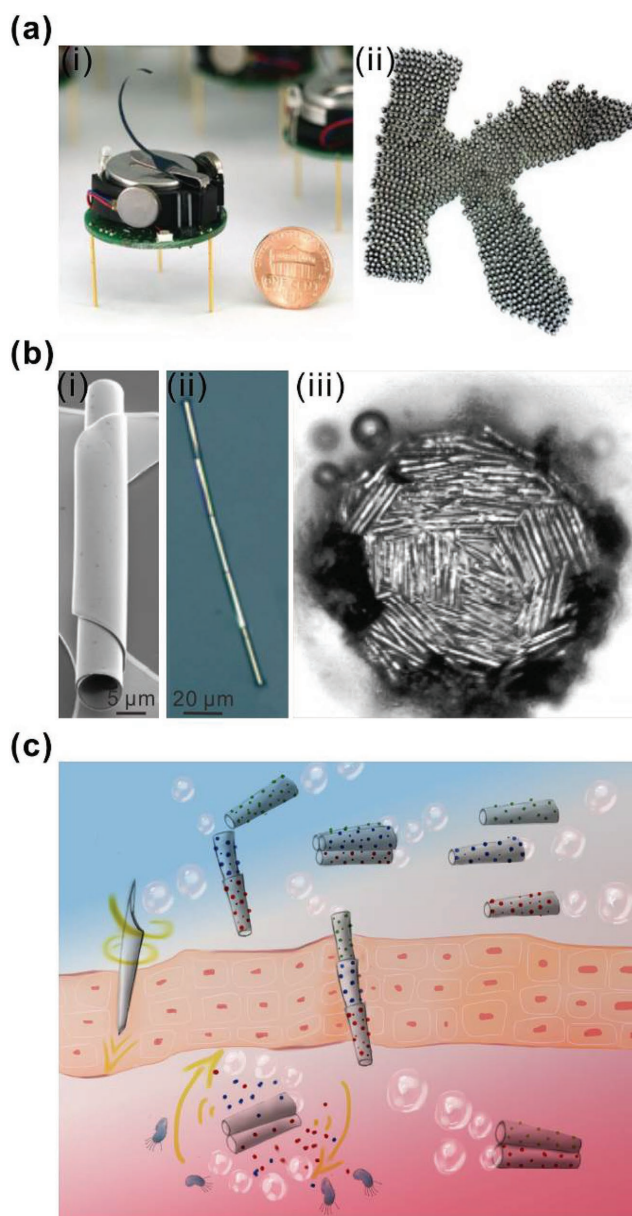


Figure 11. Intelligent transformers consisting of a team of macroscale robots and tubular micro/nanomotors. a) Thousands of macroscale robots assembled into designed shapes through their interactions. (i) Designed robot with a size similar to that of a U. S. penny. (ii) Thousands of robots assembled into the shape of the letter “K”. Reproduced with permission.^[137] Copyright 2014, AAAS. b) Self-alignment and self-assembly of tubular micro/nanomotors. (i) SEM image of a rolled-up microtube with ferromagnetic components. (ii) Five microtubes aligned through the interaction of their magnetic forces. (iii) Gathering behavior of tubular micro/nanomotors caused by capillary force. (i) and (ii) are adapted with permission.^[138] Copyright 2009, IOP Publishing Ltd. (iii) is reproduced with permission.^[139] Copyright 2013, Royal Society of Chemistry. c) Proposed sketch of transformers consisting of a team of tubular micro/nanomotors for completing different tasks on the micro-nanoscale.

reaction-driven tubular micro/nanomotors have also been developed based on biofriendly chemical reactions and external sources, and they possess infinite potential for *in vivo*

bioapplications through modification with biofriendly materials, such as Au and carbon-based materials.

With regard to the future of rocket-like tubular micro/nanomotors, their future fabrication requires a convenient method for achieving the large-scale production of specifically designed geometries. In addition, different fuels and mechanisms of propulsion, especially biocompatible fuels for in vivo applications, will be explored to generate higher thrust in various environments. Currently, tubular micro/nanomotors are typically modified to perform a single specific task, which restricts the general use of tubular micro/nanomotors. Hence, an intelligent tubular micro/nanomotor is desired that can fulfill multiple functions in a smart manner by moving and operating according to a specific design and commands. Apart from the investigations of single intelligent tubular micro/nanomotors, cooperation among a group of tubular micro/nanomotors may provide more attractive prospects. Thousands of robots have been designed at the macroscale (Figure 11a-i) to achieve the programmable formation of different shapes (Figure 11a-ii) via their local communication.^[137] Likewise, interaction between various tubular micro/nanomotors could allow them to act as transformers to complete complex tasks. To date, several interactions have been developed for assembling tubular micro/nanomotors. For example, rolled-up microtubes with a ferromagnetic component (Figure 11b-i) formed a straight line through their magnetic interactions (Figure 11b-ii).^[138] Furthermore, tubular micro/nanomotors moving at a liquid surface tend to gather together under the influence of capillary force (Figure 11b-iii).^[139] In addition, a very recent report described the organized motion of a group of microparticles.^[140] However, smart assembly and transformation are still far from being achieved. Interaction, communication, and cooperation between tubular micro/nanomotors will endow them with the ability to transform into different shapes so that they can utilize the optimal strategy to handle an assigned mission. As sketched in Figure 11c, individual tubular micromotors could assemble in parallel to generate great power for faster navigation or a stronger towing force. In addition, assembly in a line could provide better drilling behavior. If tubular micro/nanomotors could assemble such that they eject bubbles in different directions, fast rotation could be produced to accelerate the release of cargos. As in an assembly line constructed of a series of machines to autonomously produce goods with high efficiency, the realization of interaction, communication, and cooperation among tubular micro/nanomotors would tremendously improve their working efficiency and allow complicated task to be autonomously completed. We believe that the investigations of tubular micro/nanomotors and all kinds of micro/nanomachines will create a new era, much like machines did hundreds of years ago.

Acknowledgements

This work was supported by the Natural Science Foundation of China (grant nos. 51711540298, 61628401, U1632115, and 51475093), Science and Technology Commission of Shanghai Municipality (grant nos. 14JC1400200 and 17JC1401700), the National Key Technologies R&D Program of China (grant no. 2015ZX02102-003), and the Changjiang Young Scholars Program of China.

Conflict of Interest

The authors declare no conflict of interest.

Keywords

micro/nanomachines, micro/nanomotors, propulsion, tubular structures

Received: October 11, 2017

Revised: November 24, 2017

Published online: January 11, 2018

- [1] R. L. Hills, *Power from Steam: A History of the Stationary Steam Engine*, Cambridge University Press, Cambridge, UK 1989.
- [2] V. Smil, *Creating the Twentieth Century: Technical Innovations of 1867–1914 and Their Lasting Impact*, Oxford University Press, New York, New York, USA 2005.
- [3] P. R. Feynman, *Eng. Sci.* **1960**, 23, 22.
- [4] a) M. N. Popescu, S. Dietrich, M. Tasinkevych, J. Ralston, *Eur. Phys. J. E* **2010**, 31, 351; b) W. Gao, A. Pei, J. Wang, *ACS Nano* **2012**, 6, 8432; c) W. Gao, M. D'Agostino, V. Garcia-Gradilla, J. Orozco, J. Wang, *Small* **2013**, 9, 467; d) W. Gao, X. Feng, A. Pei, Y. Gu, J. Li, J. Wang, *Nanoscale* **2013**, 5, 4696; e) J. Li, V. V. Singh, S. Sattayasamitsathit, J. Orozco, K. Kaufmann, R. Dong, W. Gao, B. Jurado-Sanchez, Y. Fedorak, J. Wang, *ACS Nano* **2014**, 8, 11118; f) X. Ma, A. Jannasch, U. Albrecht, K. Hahn, A. Miguel-López, E. Schäffer, S. Sánchez, *Nano Lett.* **2015**, 15, 7043; g) D. Rojas, B. Jurado-Sánchez, A. Escarpa, *Anal. Chem.* **2016**, 88, 4153; h) Y. Yoshizumi, K. Okubo, M. Yokokawa, H. Suzuki, *Langmuir* **2016**, 32, 9381; i) D. A. Uygun, B. Jurado-Sanchez, M. Uygun, J. Wang, *Environ. Sci. Nano* **2016**, 3, 559; j) P. S. Schattling, M. A. Ramos-Docampo, V. Salgueiriño, B. Städler, *ACS Nano* **2017**, 11, 3973; k) D. Zhou, Y. C. Li, P. Xu, N. S. McCool, L. Li, W. Wang, T. E. Mallouk, *Nanoscale* **2017**, 9, 75.
- [5] a) W. F. Paxton, K. C. Kistler, C. C. Olmeda, A. Sen, S. K. St. Angelo, Y. Cao, T. E. Mallouk, P. E. Lammert, V. H. Crespi, *J. Am. Chem. Soc.* **2004**, 126, 13424; b) T. R. Kline, W. F. Paxton, T. E. Mallouk, A. Sen, *Angew. Chem., Int. Ed.* **2005**, 44, 744; c) S. Sundararajan, P. E. Lammert, A. W. Zudans, V. H. Crespi, A. Sen, *Nano Lett.* **2008**, 8, 1271; d) D. Kagan, P. Calvo-Marzal, S. Balasubramanian, S. Sattayasamitsathit, K. M. Manesh, G. Flechsig, J. Wang, *J. Am. Chem. Soc.* **2009**, 131, 12082; e) J. Wang, *ACS Nano* **2009**, 3, 4.
- [6] a) A. Ghosh, P. Fischer, *Nano Lett.* **2009**, 9, 2243; b) L. Zhang, J. J. Abbott, L. Dong, B. E. Kratochvil, D. Bell, B. J. Nelson, *Appl. Phys. Lett.* **2009**, 94, 64107; c) S. Tottori, L. Zhang, F. Qiu, K. K. Krawczyk, A. Franco-Obregón, B. J. Nelson, *Adv. Mater.* **2012**, 24, 811; d) S. Schuerle, S. Pané, E. Pellicer, J. Sort, M. D. Baró, B. J. Nelson, *Small* **2012**, 8, 1498; e) D. Schamel, A. G. Mark, J. G. Gibbs, C. Miksch, K. I. Morozov, A. M. Leshansky, P. Fischer, *ACS Nano* **2014**, 8, 8794; f) M. A. Zeeshan, R. Grisch, E. Pellicer, K. M. Sivaraman, K. E. Peyer, J. Sort, B. Özkale, M. S. Sakar, B. J. Nelson, S. Pané, *Small* **2014**, 10, 1284; g) W. Gao, X. Feng, A. Pei, C. R. Kane, R. Tam, C. Hennessy, J. Wang, *Nano Lett.* **2014**, 14, 305.
- [7] a) B. J. Williams, S. V. Anand, J. Rajagopalan, M. T. A. Saif, *Nat. Commun.* **2014**, 5, 3081; b) W. Zhu, J. Li, Y. J. Leong, I. Rozen, X. Qu, R. Dong, Z. Wu, W. Gao, P. H. Chung, J. Wang, S. Chen, *Adv. Mater.* **2015**, 27, 4411; c) B. Dai, J. Wang, Z. Xiong, X. Zhan, W. Dai, C. Li, S. Feng, J. Tang, *Nat. Nanotechnol.* **2016**, 11, 1087.
- [8] a) H. Wang, M. Pumera, *Chem. Rev.* **2015**, 115, 8704; b) S. Sánchez, L. Soler, J. Katuri, *Angew. Chem., Int. Ed.* **2015**, 54, 1414; c) K. Kim, J. Guo, X. Xu, D. L. Fan, *Small* **2015**, 11, 4037.

- [9] a) J. Wang, W. Gao, *ACS Nano* **2012**, *6*, 5745; b) B. Jurado-Sánchez, A. Escarpa, *TrAC, Trends Anal. Chem.* **2016**, *84*, 48.
- [10] a) Y. F. Mei, A. A. Solovev, S. Sanchez, O. G. Schmidt, *Chem. Soc. Rev.* **2011**, *40*, 2109; b) G. S. Huang, J. Wang, Y. F. Mei, *J. Mater. Chem.* **2012**, *22*, 6519; c) B. Xu, Y. F. Mei, *Sci. Bull.* **2017**, *62*, 525.
- [11] J. Parmar, D. Vilela, S. Sanchez, *Eur. Phys. J.: Spec. Top.* **2016**, *225*, 2255.
- [12] J. Li, I. Rozen, J. Wang, *ACS Nano* **2016**, *10*, 5619.
- [13] a) J. G. S. Moo, C. C. Mayorga-Martinez, H. Wang, B. Khezri, W. Z. Teo, M. Pumera, *Adv. Funct. Mater.* **2017**, *27*, 1604759; b) H. Ceylan, J. Giltinan, K. Kozielski, M. Sitti, *Lab Chip* **2017**, *17*, 1705.
- [14] E. M. Purcell, *Am. J. Phys.* **1977**, *45*, 3.
- [15] W. F. Paxton, S. Sundararajan, T. E. Mallouk, A. Sen, *Angew. Chem., Int. Ed.* **2006**, *45*, 5420.
- [16] a) D. L. Fan, F. Q. Zhu, R. C. Cammarata, C. L. Chien, *Appl. Phys. Lett.* **2004**, *85*, 4175; b) D. L. Fan, F. Q. Zhu, R. C. Cammarata, C. L. Chien, *Phys. Rev. Lett.* **2005**, *94*, 247208; c) G. Loget, A. Kuhn, *J. Am. Chem. Soc.* **2010**, *132*, 15918; d) P. Calvo-Marzal, S. Sattayasamitsathit, S. Balasubramanian, J. R. Windmiller, C. Dao, J. Wang, *Chem. Commun.* **2010**, *46*, 1623; e) G. Loget, A. Kuhn, *Nat. Commun.* **2011**, *2*, 535; f) G. Hwang, R. Braive, L. Couraud, A. Cavanna, O. Abdelkarim, I. Robert-Philip, A. Beveratos, I. Sagnes, S. Haliyo, S. Régnier, *Int. J. Rob. Res.* **2011**, *30*, 806.
- [17] a) R. Dreyfus, J. Baudry, M. L. Roper, M. Fermigier, H. A. Stone, J. Bibette, *Nature* **2005**, *437*, 862; b) T. Mirkovic, M. L. Foo, A. C. Arsenault, S. Fournier-Bidoz, N. S. Zacharia, G. A. Ozin, *Nat. Nanotechnol.* **2007**, *2*, 565; c) L. Zhang, T. Petit, Y. Lu, B. E. Kratochvil, K. E. Peyer, R. Pei, J. Lou, B. J. Nelson, *ACS Nano* **2010**, *4*, 6228; d) W. Gao, S. Sattayasamitsathit, K. M. Manesh, D. Weihs, J. Wang, *J. Am. Chem. Soc.* **2010**, *132*, 14403.
- [18] a) W. Wang, L. A. Castro, M. Hoyos, T. E. Mallouk, *ACS Nano* **2012**, *6*, 6122; b) Z. Wu, T. Li, J. Li, W. Gao, T. Xu, C. Christianson, W. Gao, M. Galarnyk, Q. He, L. Zhang, J. Wang, *ACS Nano* **2014**, *8*, 12041.
- [19] a) V. Magdanz, S. Sanchez, O. G. Schmidt, *Adv. Mater.* **2013**, *25*, 6581; b) M. Medina-Sánchez, L. Schwarz, A. K. Meyer, F. Hebenstreit, O. G. Schmidt, *Nano Lett.* **2016**, *16*, 555; c) M. M. Stanton, B. Park, A. Miguel-López, X. Ma, M. Sitti, S. Sánchez, *Small* **2017**, *13*, 1603679.
- [20] a) R. Golestanian, T. B. Liverpool, A. Ajdari, *New J. Phys.* **2007**, *9*, 126; b) M. N. Popescu, S. Dietrich, M. Tasinkevych, J. Ralston, *Eur. Phys. J. E: Soft Matter Biol. Phys.* **2010**, *31*, 351.
- [21] a) Y. Wang, R. M. Hernandez, D. J. Bartlett, J. M. Bingham, T. R. Kline, A. Sen, T. E. Mallouk, *Langmuir* **2006**, *22*, 10451; b) R. Liu, A. Sen, *J. Am. Chem. Soc.* **2011**, *133*, 20064; c) T. Lee, M. Alarcón-Correa, C. Miksch, K. Hahn, J. G. Gibbs, P. Fischer, *Nano Lett.* **2014**, *14*, 2407; d) R. Dong, Q. Zhang, W. Gao, A. Pei, B. Ren, *ACS Nano* **2016**, *10*, 839.
- [22] J. G. Gibbs, Y. P. Zhao, *Appl. Phys. Lett.* **2009**, *94*, 163104.
- [23] A. A. Solovev, Y. F. Mei, E. Bermúdez Ureña, G. S. Huang, O. G. Schmidt, *Small* **2009**, *5*, 1688.
- [24] Y. F. Mei, G. S. Huang, A. A. Solovev, E. B. Ureña, I. Mönch, F. Ding, T. Reindl, R. K. Y. Fu, P. K. Chu, O. G. Schmidt, *Adv. Mater.* **2008**, *20*, 4085.
- [25] V. M. Fomin, M. Hippler, V. Magdanz, L. Soler, S. Sanchez, O. G. Schmidt, *IEEE Trans. Rob.* **2014**, *30*, 40.
- [26] H. C. Berg, R. A. Anderson, *Nature* **1973**, *245*, 380.
- [27] M. L. Depamphi, J. Adler, *J. Bacteriol.* **1971**, *105*, 384.
- [28] T. Iino, M. Mitani, *J. Gen. Microbiol.* **1967**, *49*, 81.
- [29] J. Li, G. S. Huang, M. Ye, M. Li, R. Liu, Y. F. Mei, *Nanoscale* **2011**, *3*, 5083.
- [30] a) J. Li, G. S. Huang, M. Ye, M. Li, R. Liu, Y. F. Mei, *Nanoscale* **2011**, *3*, 5083; b) M. Manjare, B. Yang, Y. P. Zhao, *J. Phys. Chem. C* **2013**, *117*, 4657; c) B. Sarkis, D. Folio, A. Ferreira, *IEEE Int. Conf. Robotics and Automation (ICRA)*, IEEE Computer Soc, Seattle, WA, USA, **2015**, p. 3537.
- [31] L. Li, J. Wang, T. Li, W. Song, G. Zhang, *Soft Matter* **2014**, *10*, 7511.
- [32] S. Sattayasamitsathit, H. Kou, W. Gao, W. Thavarajah, K. Kaufmann, L. Zhang, J. Wang, *Small* **2014**, *10*, 2830.
- [33] L. Li, J. Wang, T. Li, W. Song, G. Zhang, *J. Appl. Phys.* **2015**, *117*, 104308.
- [34] a) T. G. Leong, A. M. Zarafshar, D. H. Gracias, *Small* **2010**, *6*, 792; b) Z. Liu, J. Li, B. Lu, Y. Chen, R. Liu, G. S. Huang, Y. F. Mei, *J. Vac. Sci. Technol.* **2013**, *31*, 011806; c) F. Cavallo, M. G. Lagally, *Nano Today* **2015**, *10*, 538; d) J. Zhang, J. Li, S. Tang, Y. Fang, J. Wang, G. S. Huang, R. Liu, L. Zheng, X. Cui, Y. F. Mei, *Sci. Rep.* **2015**, *5*, 15012; e) Q. Guo, M. Zhang, Z. Xue, J. Zhang, G. Wang, D. Chen, Z. Mu, G. S. Huang, Y. F. Mei, Z. Di, X. Wang, *AIP Adv.* **2015**, *5*, 037115; f) J. Rogers, Y. Huang, O. G. Schmidt, D. H. Gracias, *MRS Bull.* **2016**, *41*, 123; g) X. Lin, Y. Fang, L. Zhu, J. Zhang, G. S. Huang, J. Wang, Y. F. Mei, *Adv. Opt. Mater.* **2016**, *4*, 936; h) H. Wang, H. Zhen, S. Li, Y. Jing, G. S. Huang, Y. F. Mei, W. Lu, *Sci. Adv.* **2016**, *2*, e1600027; i) Y. Zhang, F. Zhang, Z. Yan, Q. Ma, X. Li, Y. Huang, J. A. Rogers, *Nat. Rev. Mater.* **2017**, *2*, 17019; j) L. Xu, T. C. Shyu, N. A. Kotov, *ACS Nano* **2017**, *11*, 7587.
- [35] a) V. Y. Prinz, V. A. Seleznev, A. K. Gutakovskiy, A. V. Chehovskiy, V. V. Preobrazhenskii, M. A. δ. G. Putyato, *Physica E* **2000**, *6*, 828; b) O. G. Schmidt, K. Eberl, *Nature* **2001**, *410*, 168.
- [36] a) X. Li, *Adv. Opt. Photonics* **2011**, *3*, 366; b) J. Wang, T. Zhan, G. S. Huang, X. Cui, X. Hu, Y. F. Mei, *Opt. Express* **2012**, *20*, 18555; c) G. Wan, A. A. Solovev, G. S. Huang, M. F. Maitz, N. Huang, Y. F. Mei, *J. Mater. Chem.* **2012**, *22*, 12983; d) J. Li, Z. Liu, B. Lu, G. S. Huang, Y. Chen, Y. F. Mei, R. Liu, *Microelectron. Eng.* **2012**, *98*, 623; e) G. S. Huang, Y. F. Mei, *Adv. Mater.* **2012**, *24*, 2517; f) J. Zhong, J. Wang, G. S. Huang, G. Yuan, Y. F. Mei, *Nanoscale Res. Lett.* **2013**, *8*, 531; g) J. Zhang, J. Zhong, Y. Fang, J. Wang, G. S. Huang, X. Cui, Y. F. Mei, *Nanoscale* **2014**, *6*, 13646; h) J. Wang, T. Zhan, G. S. Huang, P. K. Chu, Y. F. Mei, *Laser Photonics Rev.* **2014**, *8*, 521; i) Y. Zhang, D. Han, D. Du, G. S. Huang, T. Qiu, Y. F. Mei, *Plasmonics* **2015**, *10*, 949.
- [37] K. Yao, M. Manjare, C. A. Barrett, B. Yang, T. T. Salguero, Y. Zhao, *J. Phys. Chem. Lett.* **2012**, *3*, 2204.
- [38] J. Li, J. Zhang, W. Gao, G. S. Huang, Z. Di, R. Liu, J. Wang, Y. F. Mei, *Adv. Mater.* **2013**, *25*, 3715.
- [39] G. Zhao, A. Ambrosi, M. Pumera, *J. Mater. Chem. A* **2014**, *2*, 1219.
- [40] H. Wang, J. G. S. Moo, M. Pumera, *Nanoscale* **2014**, *6*, 11359.
- [41] a) G. P. Nikishkov, *J. Appl. Phys.* **2003**, *94*, 5333; b) J. Zang, F. Liu, *Appl. Phys. Lett.* **2008**, *92*, 21905; c) I. S. Chun, A. Challa, B. Derickson, K. J. Hsia, X. Li, *Nano Lett.* **2010**, *10*, 3927; d) S. Alben, B. Balakrisnan, E. Smela, *Nano Lett.* **2011**, *11*, 2280; e) Z. Chen, G. S. Huang, I. Trase, X. Han, Y. F. Mei, *Phys. Rev. Appl.* **2016**, *5*, 017001. f) Z. Tian, L. Zhang, Y. Fang, B. Xu, S. Tang, N. Hu, Z. An, Z. Chen, Y. F. Mei, *Adv. Mater.* **2017**, *29*, 1604572.
- [42] M. Bognitzki, H. Q. Hou, M. Ishaque, T. Frese, M. Hellwig, C. Schwarte, A. Schaper, J. H. Wendorff, A. Greiner, *Adv. Mater.* **2000**, *12*, 637.
- [43] J. Goldberger, R. R. He, Y. F. Zhang, S. W. Lee, H. Q. Yan, H. J. Choi, P. D. Yang, *Nature* **2003**, *422*, 599.
- [44] K. M. Manesh, M. Cardona, R. Yuan, M. Clark, D. Kagan, S. Balasubramanian, J. Wang, *ACS Nano* **2010**, *4*, 1799.
- [45] Z. Dong, C. Jiang, H. Cheng, Y. Zhao, G. Shi, L. Jiang, L. Qu, *Adv. Mater.* **2012**, *24*, 1856.
- [46] C. Hu, Y. Zhao, H. Cheng, Y. Wang, Z. Dong, C. Jiang, X. Zhai, L. Jiang, L. Qu, *Nano Lett.* **2012**, *12*, 5879.
- [47] P. Sozzani, S. Bracco, A. Comotti, R. Simonutti, P. Valsesia, Y. Sakamoto, O. Terasaki, *Nature* **2006**, *5*, 545.
- [48] W. Gao, S. Sattayasamitsathit, J. Orozco, J. Wang, *J. Am. Chem. Soc.* **2011**, *133*, 11862.

- [49] G. Zhao, M. Pumera, *RSC Adv.* **2013**, *3*, 3963.
- [50] A. Martín, B. Jurado-Sánchez, A. Escarpa, J. Wang, *Small* **2015**, *11*, 3568.
- [51] R. Maria-Hormigos, B. Jurado-Sanchez, L. Vazquez, A. Escarpa, *Chem. Mater.* **2016**, *28*, 8962.
- [52] Z. Wu, Y. Wu, W. He, X. Lin, J. Sun, Q. He, *Angew. Chem., Int. Ed.* **2013**, *52*, 7000.
- [53] G. Zhao, A. Ambrosi, M. Pumera, *Nanoscale* **2013**, *5*, 1319.
- [54] J. Li, W. Liu, J. Wang, I. Rozen, S. He, C. Chen, H. G. Kim, H. Lee, H. Lee, S. Kwon, T. Li, L. Li, J. Wang, Y. F. Mei, *Adv. Funct. Mater.* **2017**, *27*, 1700598.
- [55] a) M. P. Stoykovich, H. Kang, K. C. Daoulas, G. Liu, C. Liu, J. J. de Pablo, M. Müller, P. F. Nealey, *ACS Nano* **2007**, *1*, 168; b) J. Bang, U. Jeong, D. Y. Ryu, T. P. Russell, C. J. Hawker, *Adv. Mater.* **2009**, *21*, 4769; c) C. Lin, S. Polisetty, L. O'Brien, A. Baruth, M. A. Hillmyer, C. Leighton, W. L. Gladfelter, *ACS Nano* **2015**, *9*, 1379.
- [56] Y. Li, Y. Fang, J. Wang, L. Wang, S. Tang, C. Jiang, L. Zheng, Y. F. Mei, *Lab Chip* **2016**, *16*, 4406.
- [57] W. Gao, S. Sattayasamitsathit, J. Wang, *Chem. Rec.* **2012**, *12*, 224.
- [58] H. Wang, J. G. S. Moo, M. Pumera, *ACS Nano* **2016**, *10*, 5041.
- [59] C. Jiang, G. S. Huang, S. Ding, H. Dong, C. Men, Y. F. Mei, *Nanoscale Res. Lett.* **2016**, *11*, 289.
- [60] J. Li, Z. Liu, G. S. Huang, Z. An, G. Chen, J. Zhang, M. Li, R. Liu, Y. F. Mei, *NPG Asia Mater.* **2014**, *6*, e94.
- [61] W. Gao, S. Sattayasamitsathit, A. Uygun, A. Pei, A. Ponedal, J. Wang, *Nanoscale* **2012**, *4*, 2447.
- [62] S. Sanchez, A. N. Ananth, V. M. Fomin, M. Viehriig, O. G. Schmidt, *J. Am. Chem. Soc.* **2011**, *133*, 14860.
- [63] a) H. Wang, G. Zhao, M. Pumera, *J. Phys. Chem. C* **2014**, *118*, 5268; b) J. Simmchen, V. Magdanz, S. Sanchez, S. Chokmaviroj, D. Ruiz-Molina, A. Baeza, O. G. Schmidt, *RSC Adv.* **2014**, *4*, 20334.
- [64] J. G. S. Moo, H. Wang, M. Pumera, *Chem. - Eur. J.* **2016**, *22*, 355.
- [65] S. Sanchez, A. A. Solovev, S. M. Harazim, C. Deneke, Y. F. Mei, O. G. Schmidt, *Chem. Rec.* **2011**, *11*, 367.
- [66] J. Li, B. Lu, Z. Shen, Z. Xu, H. Li, J. Wen, Z. Li, X. Qu, Y. Chen, Y. F. Mei, R. Liu, *Microelectron. Eng.* **2011**, *88*, 1792.
- [67] a) I. S. M. Khalil, V. Magdanz, S. Sanchez, O. G. Schmidt, S. Misra, *Appl. Phys. Lett.* **2013**, *103*, 172404; b) I. S. M. Khalil, V. Magdanz, S. Sanchez, O. G. Schmidt, S. Misra, *IEEE Trans. Rob.* **2014**, *30*, 49.
- [68] G. Zhao, S. Sanchez, O. G. Schmidt, M. Pumera, *Chem. Commun.* **2012**, *48*, 10090.
- [69] A. A. Solovev, E. J. Smith, C. C. Bof Bufon, S. Sanchez, O. G. Schmidt, *Angew. Chem., Int. Ed.* **2011**, *50*, 10875.
- [70] Z. Liu, J. Li, J. Wang, G. S. Huang, R. Liu, Y. F. Mei, *Nanoscale* **2013**, *5*, 1345.
- [71] Z. Wu, X. Lin, Y. Wu, T. Si, J. Sun, Q. He, *ACS Nano* **2014**, *8*, 6097.
- [72] F. Mou, Y. Li, C. Chen, W. Li, Y. Yin, H. Ma, J. Guan, *Small* **2015**, *11*, 2564.
- [73] J. G. S. Moo, S. Presolski, M. Pumera, *ACS Nano* **2016**, *10*, 3543.
- [74] T. Xu, F. Soto, W. Gao, V. Garcia-Gradilla, J. Li, X. Zhang, J. Wang, *J. Am. Chem. Soc.* **2014**, *136*, 8552.
- [75] L. Restrepo-Perez, L. Soler, C. S. Martinez-Cisneros, S. Sanchez, O. G. Schmidt, *Lab Chip* **2014**, *14*, 1515.
- [76] V. Magdanz, G. Stoychev, L. Ionov, S. Sanchez, O. G. Schmidt, *Angew. Chem., Int. Ed.* **2014**, *53*, 2673.
- [77] A. Jodra, F. Soto, M. A. Lopez-Ramirez, A. Escarpa, J. Wang, *Chem. Commun.* **2016**, *52*, 11838.
- [78] W. Z. Teo, H. Wang, M. Pumera, *Chem. Commun.* **2016**, *52*, 4333.
- [79] M. Safdar, O. M. Wani, J. Jänis, *ACS Appl. Mater. Interfaces* **2015**, *7*, 25580.
- [80] T. D. Minh, M. Safdar, J. Jänis, *Chem. - Eur. J.* **2017**, *23*, 8134.
- [81] S. Sanchez, A. A. Solovev, Y. F. Mei, O. G. Schmidt, *J. Am. Chem. Soc.* **2010**, *132*, 13144.
- [82] X. Ma, A. C. Hortelao, A. Miguel-López, S. Sánchez, *J. Am. Chem. Soc.* **2016**, *138*, 13782.
- [83] G. Zhao, H. Wang, B. Khezri, R. D. Webster, M. Pumera, *Lab Chip* **2013**, *13*, 2937.
- [84] a) G. Zhao, M. Viehriig, M. Pumera, *Lab Chip* **2013**, *13*, 1930; b) H. Wang, G. Zhao, M. Pumera, *Phys. Chem. Chem. Phys.* **2013**, *15*, 17277.
- [85] L. Soler, C. Martinez-Cisneros, A. Swiers, S. Sanchez, O. G. Schmidt, *Lab Chip* **2013**, *13*, 4299.
- [86] A. A. Solovev, S. Sanchez, M. Pumera, Y. F. Mei, O. G. Schmidt, *Adv. Funct. Mater.* **2010**, *20*, 2430.
- [87] A. A. Solovev, Y. F. Mei, O. G. Schmidt, *Adv. Mater.* **2010**, *22*, 4340.
- [88] a) S. Sanchez, A. A. Solovev, S. M. Harazim, O. G. Schmidt, *J. Am. Chem. Soc.* **2011**, *133*, 701; b) S. Sanchez, A. A. Solovev, S. Schulze, O. G. Schmidt, *Chem. Commun.* **2011**, *47*, 698.
- [89] D. Kagan, S. Campuzano, S. Balasubramanian, F. Kuralay, G. Flechsig, J. Wang, *Nano Lett.* **2011**, *11*, 2083.
- [90] L. Restrepo-Perez, L. Soler, C. Martinez-Cisneros, S. Sanchez, O. G. Schmidt, *Lab Chip* **2014**, *14*, 2914.
- [91] J. Orozco, A. Cortés, G. Cheng, S. Sattayasamitsathit, W. Gao, X. Feng, Y. Shen, J. Wang, *J. Am. Chem. Soc.* **2013**, *135*, 5336.
- [92] J. Orozco, G. Pan, S. Sattayasamitsathit, M. Galarnyk, J. Wang, *Analyst* **2015**, *140*, 1421.
- [93] S. Balasubramanian, D. Kagan, C. Jack Hu, S. Campuzano, M. J. Lobo-Castañón, N. Lim, D. Y. Kang, M. Zimmerman, L. Zhang, J. Wang, *Angew. Chem., Int. Ed.* **2011**, *50*, 4161.
- [94] Z. Wu, X. Lin, X. Zou, J. Sun, Q. He, *ACS Appl. Mater. Interfaces* **2015**, *7*, 250.
- [95] J. Orozco, S. Campuzano, D. Kagan, M. Zhou, W. Gao, J. Wang, *Anal. Chem.* **2011**, *83*, 7962.
- [96] S. Campuzano, J. Orozco, D. Kagan, M. Guix, W. Gao, S. Sattayasamitsathit, J. C. Claussen, A. Merkoçi, J. Wang, *Nano Lett.* **2012**, *12*, 396.
- [97] F. Kuralay, S. Sattayasamitsathit, W. Gao, A. Uygun, A. Katzenberg, J. Wang, *J. Am. Chem. Soc.* **2012**, *134*, 15217.
- [98] A. A. Solovev, W. Xi, D. H. Gracias, S. M. Harazim, C. Deneke, S. Sanchez, O. G. Schmidt, *ACS Nano* **2012**, *6*, 1751.
- [99] W. Xi, A. A. Solovev, A. N. Ananth, D. H. Gracias, S. Sanchez, O. G. Schmidt, *Nanoscale* **2013**, *5*, 1294.
- [100] M. García, J. Orozco, M. Guix, W. Gao, S. Sattayasamitsathit, A. Escarpa, A. Merkoçi, J. Wang, *Nanoscale* **2013**, *5*, 1325.
- [101] D. Vilela, J. Orozco, G. Cheng, S. Sattayasamitsathit, M. Galarnyk, C. Kan, J. Wang, A. Escarpa, *Lab Chip* **2014**, *14*, 3505.
- [102] X. Yu, Y. Li, J. Wu, H. Ju, *Anal. Chem.* **2014**, *86*, 4501.
- [103] J. Orozco, V. García-Gradilla, M. D. Agostino, W. Gao, A. Cortés, J. Wang, *ACS Nano* **2013**, *7*, 818.
- [104] V. V. Singh, K. Kaufmann, B. Esteban-Fernández De Ávila, M. Uygun, J. Wang, *Chem. Commun.* **2016**, *52*, 3360.
- [105] V. N. Khiem, S. D. Minteer, *Chem. Commun.* **2015**, *51*, 4782.
- [106] Y. Xie, S. Fu, J. Wu, J. Lei, H. Ju, *Biosens. Bioelectron.* **2017**, *87*, 31.
- [107] B. Jurado-Sánchez, A. Escarpa, J. Wang, *Chem. Commun.* **2015**, *51*, 14088.
- [108] B. Esteban-Fernández De Ávila, M. A. Lopez-Ramirez, D. F. Báez, A. Jodra, V. V. Singh, K. Kaufmann, J. Wang, *ACS Sens.* **2016**, *1*, 217.
- [109] R. Maria-Hormigos, B. Jurado-Sánchez, A. Escarpa, *Nanoscale* **2017**, *9*, 6286.
- [110] E. Morales-Narváez, M. Guix, M. Medina-Sánchez, C. C. Mayorga-Martinez, A. Merkoçi, *Small* **2014**, *10*, 2542.
- [111] D. Han, Y. Fang, D. Du, G. S. Huang, T. Qiu, Y. F. Mei, *Nanoscale* **2016**, *8*, 9141.
- [112] a) L. Soler, S. Sanchez, *Nanoscale* **2014**, *6*, 7175; b) W. Gao, J. Wang, *ACS Nano* **2014**, *8*, 3170.
- [113] M. Guix, J. Orozco, M. García, W. Gao, S. Sattayasamitsathit, A. Merkoçi, A. Escarpa, J. Wang, *ACS Nano* **2012**, *6*, 4445.
- [114] T. Li, L. Li, W. Song, L. Wang, G. Shao, G. Zhang, *ECS J. Solid State Sci. Technol.* **2015**, *4*, S3016.

- [115] V. V. Singh, A. Martin, K. Kaufmann, S. D. S. De Oliveira, J. Wang, *Chem. Mater.* **2015**, *27*, 8162.
- [116] D. Vilela, J. Parmar, Y. Zeng, Y. Zhao, S. Sánchez, *Nano Lett.* **2016**, *16*, 2860.
- [117] L. Soler, V. Magdanz, V. M. Fomin, S. Sanchez, O. G. Schmidt, *ACS Nano* **2013**, *7*, 9611.
- [118] J. Parmar, D. Vilela, E. Pellicer, D. Esqué-de Los Ojos, J. Sort, S. Sánchez, *Adv. Funct. Mater.* **2016**, *26*, 4152.
- [119] J. Orozco, G. Cheng, D. Vilela, S. Sattayasamitsathit, R. Vazquez-Duhalt, G. Valdés-Ramírez, O. S. Pak, A. Escarpa, C. Kan, J. Wang, *Angew. Chem., Int. Ed.* **2013**, *52*, 13276.
- [120] M. Uygun, V. V. Singh, K. Kaufmann, D. A. Uygun, S. D. S. de Oliveira, J. Wang, *Angew. Chem., Int. Ed.* **2015**, *54*, 12900.
- [121] S. K. Srivastava, M. Guix, O. G. Schmidt, *Nano Lett.* **2016**, *16*, 817.
- [122] F. Mushtaq, A. Asani, M. Hoop, X. Chen, D. Ahmed, B. J. Nelson, S. Pané, *Adv. Funct. Mater.* **2016**, *26*, 6995.
- [123] B. Jurado-Sánchez, J. Wang, A. Escarpa, *ACS Appl. Mater. Interfaces* **2016**, *8*, 19618.
- [124] W. Gao, A. Uygun, J. Wang, *J. Am. Chem. Soc.* **2012**, *134*, 897.
- [125] W. Gao, R. Dong, S. Thamphiwatana, J. Li, W. Gao, L. Zhang, J. Wang, *ACS Nano* **2015**, *9*, 117.
- [126] E. Karshalev, C. Chen, G. Marolt, A. Martín, I. Campos, R. Castillo, T. Wu, J. Wang, *Small* **2017**, *13*, 1700035.
- [127] J. Li, S. Thamphiwatana, W. Liu, B. Esteban-Fernández De Ávila, P. Angsantikul, E. Sandraz, J. Wang, T. Xu, F. Soto, V. Ramez, X. Wang, W. Gao, L. Zhang, J. Wang, *ACS Nano* **2016**, *10*, 9536.
- [128] a) V. Magdanz, O. G. Schmidt, *Expert Opin. Drug Delivery* **2014**, *11*, 1125; b) V. Magdanz, M. Medina-Sánchez, L. Schwarz, H. Xu, J. Elgeti, O. G. Schmidt, *Adv. Mater.* **2017**, *29*, 1606301; c) L. Schwarz, M. Medina-Sánchez, O. G. Schmidt, *Appl. Phys. Rev.* **2017**, *4*, 31301; d) M. Medina-Sánchez, O. G. Schmidt, *Nature* **2017**, *545*, 406.
- [129] I. S. M. Khalil, V. Magdanz, S. Sanchez, O. G. Schmidt, S. Misra, *J. Micro-Bio Rob.* **2014**, *9*, 79.
- [130] V. Magdanz, M. Medina-Sánchez, Y. Chen, M. Guix, O. G. Schmidt, *Adv. Funct. Mater.* **2015**, *25*, 2763.
- [131] V. Magdanz, M. Guix, F. Hebenstreit, O. G. Schmidt, *Adv. Mater.* **2016**, *28*, 4084.
- [132] M. Medina-Sánchez, O. G. Schmidt, *Nature* **2017**, *545*, 406.
- [133] J. Orozco, D. Vilela, G. Valdés-Ramírez, Y. Fedorak, A. Escarpa, R. Vazquez-Duhalt, J. Wang, *Chem. - Eur. J.* **2014**, *20*, 2866.
- [134] Z. Wu, T. Si, W. Gao, X. Lin, J. Wang, Q. He, *Small* **2016**, *12*, 577.
- [135] Q. Rao, T. Si, Z. Wu, M. Xuan, Q. He, *Sci. Rep.* **2017**, *7*, 4621.
- [136] J. Li, B. E. Ávila, W. Gao, L. Zhang, J. Wang, *Sci. Rob.* **2017**, *2*, eaam6431.
- [137] M. Rubenstein, A. Cornejo, R. Nagpal, *Science* **2014**, *345*, 795.
- [138] E. B. Urena, Y. F. Mei, E. Coric, D. Makarov, M. Albrecht, O. G. Schmidt, *J. Phys. D: Appl. Phys.* **2009**, *42*, 055001.
- [139] A. A. Solovev, S. Sanchez, O. G. Schmidt, *Nanoscale* **2013**, *5*, 1284.
- [140] D. Ahmed, T. Baasch, N. Blondel, N. Läubli, J. Dual, B. J. Nelson, *Nat. Commun.* **2017**, *8*, 770.